TNF

Technisch-Naturwissenschaftliche
Fakultät

Diodes with organic Schottky junctions

DIPLOMARBEIT

zur Erlangung des akademischen Grades

Diplom Ingenieurin

im Diplomstudium

WIRTSCHAFTSINGENIEURWESEN - TECHNISCHE CHEMIE

Eingereicht von:
Stefanie Schlager

Angefertigt am:
Linz Institute for Organic Solar Cells (LIOS)

Beurteilung:
o. Univ. Prof. Dr. Serdar N. Sariciftci

Mitwirkung:
Dr. Philipp Stadler
Dr. Matthew White

Linz, Oktober 2011

Acknowledgement

Diodes with organic Schottky junctions

Abstract

This study uses organic semiconductors with good optical properties (used for organic solar cells) capped with different low work-function metals as the foundation for constructing Schottky diodes. Poly-(3-hexylthiophene) (P3HT), poly-[2-methoxy-5-(3', 7'-dimethyloctyl)-p-phenylene vinylene] (MDMO-PPV) and zinc phtalocyanine (ZnPc) are well known for acting as electron donor in organic bulk-heterojunction solar cells with favourable absorption properties in the visible range of light. They can be doped, e.g. by simple air exposure or by molecular doping adding iodine or charge transfer complexes such as 2,3,5,6-tetrafluoro-7,7',8,8'-tetracyanoquniodimethane (F4TCNQ). In this study a pathway to induce a controllable amount of charge carriers is shown, in order to form a Schottky barrier between the organic semiconductor and the contact electrode. Fluorinated alkyl-chains are applied to the purified intrinsic organic semiconductor thin films. These samples are capped with different low work-function metals [6]. Current-voltage characteristics with and without light application [19] as well as impedance measurements at different frequencies in dark and light were recorded. In addition the controllability of the doping method is investigated with Fourier transform infrared spectroscopy. The results from the dielectric spectroscopy of these structures were studied with Mott-Schottky analysis. The creation of chemical and photo-induced charge carriers is shown. It is expected that this idea can be applied to the elaboration of a photo-induced Schottky-barrier and further in photovoltaic devices as well.

Dioden mit organischen Schottky Kontakten

Zusammenfassung

In dieser Arbeit werden als Grundlage zur Konstruktion von Schottky Dioden organische Halbleiter mit guten optischen Eigenschaften (Verwendung für organische Solarzellen) mit verschiedenen Metallen mit niedriger Austrittsarbeit kombiniert. Poly-(3-hexylthiophen) (P3HT), poly-[2-methoxy-5-(3', 7'-dimethyloctyl)-p-phenylen vinylen] (MDMO-PPV) und Zink Phtalocyanin (ZnPc) sind bekannt für ihre Anwendung als Elektronendonoren in organischen Solarzellen, da sie vorteilhafte Absorptionseigenschaften im sichtbaren Bereich des Lichtes aufweisen. Diese organischen Halbleiter können dotiert werden wie zum Beispiel durch einfache Lufteinwirkung oder durch molekulare Dotierung durch Iod oder einen Ladungstransferkomplex wie 2,3,5,6-tetrafluoro-7,7',8,8'-tetracyanoquniodimethan (F4-TCNQ). In dieser Studie wird gezeigt wie eine kontrollierte Menge an Ladungsträgern erreicht wird, um eine Schottky Barriere zwischen organischem Halbleiter und der Kontakelektrode zu bilden. Fluorinierte Alkyl-Ketten werden in intrinsische, organische Halbleiter-Dünnschichten eingebracht. Die Proben werden dann mit verschieden Metallen mit niedriger Austrittsarbeit kombiniert [6]. Strom-Spannungs Eigenschaften mit und ohne Lichteinwirkung [19] sowie Impedanz Messungen bei verschiedenen Frequenzen und ebenfalls mit und ohne Lichteinwirkung werden untersucht. Weiters wird die Dotierung auf ihre Kontrollierbarkeit mittels Fourier transform Infrarot Spektroskopie untersucht. Die Ergebnisse der Impedanz-Spekroskopie werden in einer Mott-Schottky Analyse ausgewertet. Die Bildung von chemischen und lichtinduzierten Ladungsträgern wird gezeigt. Es wird erwartet dass dieses Konzept für die nähere Ausführung von photo-induzierten Schottky Barrieren und weiters für photovoltaische Elemente verwendet werden kann.

Contents

Contents

List of Figures

List of Figures

List of Tables

1 Introduction

1.1 Background

A potential barrier at a metal-semiconductor (MS) junction, showing a voltage drop, is called Schottky barrier. This barrier is named after Walter Schottky who developed in 1938 a model of MS devices.

For a MS-system with an intrinsic semiconductor there is simply an interface observed as shown in figure 1.1.1. This systems depicts a metal-insulator-metal (MIM) scheme. The Fermi levels of the metals and the semiconductor are aligned and the vacuum level correlates with the change of the work functions Φ_M. The Fermi levels are defined as chemical potentials in the electrons' Fermi-Dirac statistics that gives the probability of an electron to be in a single-particle state with a distinct energy. Because of missing free charges in the intrinsic semiconductor, the field distribution is homogenous and valence band and conduction band of the semiconductor, respectively HOMO (highest occupied molecular orbital) and LUMO (lowest unoccupied molecular orbital) for organic semiconductors, decrease linearly featured in figure 1.1.1.
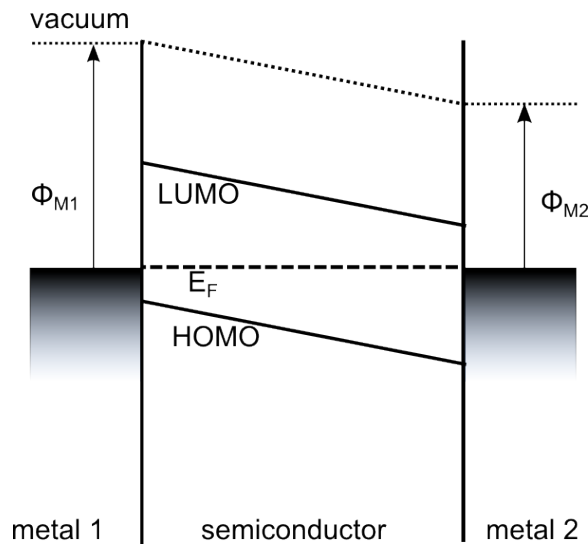
Figure 1.1.1: Energy diagram of a system with two different metals and an intrinsic semiconductor (MIM), no Schottky barrier is formed

Schottky postulated that the rectification of a MS-device is dependent from the space charge in the semiconductor. This means the characteristics of the MS-junction correspond to the doping concentration N in the semiconductor [20]. When the semiconductor in a MS-system is doped, a barrier is formed at the MS-interface as presented in figure 1.1.2. In this study only p-type doping will be discussed.
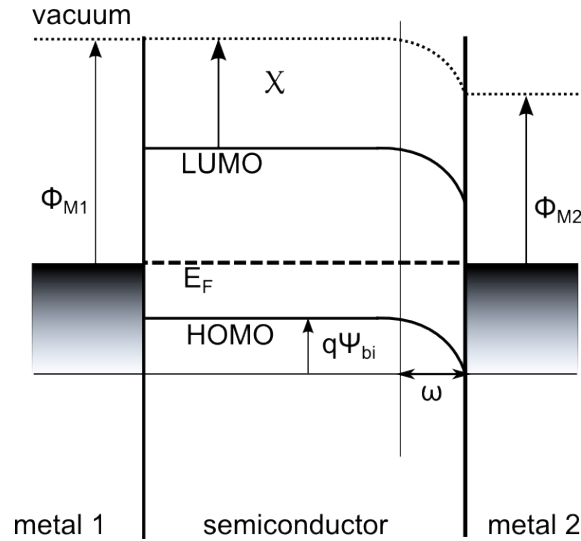
Figure 1.1.2:   Energy diagram of a system of two different metals and a p-doped semiconductor, a broad depletion width ω and the built in potential ψ_{bi} characterize the Schottky barrier between semiconductor and metal 2

The field distribution now is inhomogenous due to mobile charges generated through doping. That charges can move in the electric field. To reach equilibrium charges move across the interface of metal and semiconductor and majority carriers (positive charge carriers for p-type semiconductor) are depleted from the semiconductor in the region near to the interface. An abrupt space charge region is formed. The electric field then is compensated. At the metal-semiconductor contact a potential drop of HOMO and LUMO is observed. This drop is defined as the depletion width of the barrier and is dependent from the charge carrier concentration N_A (acceptor concentration for p-type semiconductor) in the semiconductor and from the charge carrier distribution. Assuming uniform charge carrier distribution over the bulk, which is usually the case in most semiconductors (Coulomb repulsion prevents the formation of an inhomogenous charge distribution and is defined as

$$E_C = \frac{q_1 q_2}{4\pi\varepsilon_0} \cdot \frac{1}{r} \tag{1.1.1}$$

[3]), we get for the charge density ρ

$$\rho = \begin{cases} qN_A & 0 < x < \omega \\ 0 & \omega < x \end{cases} \tag{1.1.2}$$

and for the potential drop at the interface

$$\Psi = V_{applied} - \Psi_{bi} \tag{1.1.3}$$

Assuming complete ionization and estimate the number of holes and electrons equal zero we get with the Poisson equation

$$\frac{d^2\Psi_i}{dx^2} = \frac{dE}{dx} = \frac{qN_A}{\varepsilon_S} \tag{1.1.4}$$

The electric field at the barrier is obtained by integration.

$$E(x) = \frac{qN_A(x + \omega)}{\varepsilon_S} \tag{1.1.5}$$

The maximum existing field at x=0 is defined by

$$|E_m| = \frac{qN_A\omega}{\varepsilon_S} \tag{1.1.6}$$

Integrating equation 1.1.4 two times results in the potential distribution

$$\Psi_i(x) = \frac{qN_A}{2\varepsilon_S}(x + \omega)^2 \tag{1.1.7}$$

Now the potential across the region can be written as

$$\Psi_p = \frac{qN_A\omega^2}{2\varepsilon_S} \tag{1.1.8}$$

Combining equation 1.1.6 and 1.1.8 the maximum field can also be expressed as

$$|E_m| = \sqrt{\frac{2qN_A\Psi}{\varepsilon_S}} \tag{1.1.9}$$

If we rearrange equation 1.1.8 and combine it with equation 1.1.3 we get for the depletion width

$$\omega = \sqrt{\frac{2\varepsilon_S\Psi_{bi}}{qN_A}} \tag{1.1.10}$$

For a MS-contact with a p-type semiconductor under the one-sided abrupt junction approximation a correction factor $\frac{kT}{q}$ has to be included. This term arises from the contribution of the majority-carrier distribution, in our case positive charge carriers. Therefore we obtain for the depletion width equation 1.1.11.

$$\omega = \sqrt{\frac{2\varepsilon_S}{qN_A}\left(\Psi_{bi} - V_{applied} - \frac{kT}{q}\right)} \tag{1.1.11}$$

From the voltage dependent formula for the depletion width (equation 1.1.11) it is clear that the depletion width expands under reverse bias. Under forward bias the depletion region is reduced, eventually to nothing and carriers can flow freely through the device.

To identify a junction as a Schottky junction, the charge carrier concentration N_A has to be constant respectively homogenous in the depletion region.

If N_A is constant a plot of $1/C^2$ versus voltage from the impedance measurement is expected to show a linear regime. This way to plot data from impedance measurement is called Mott Schottky analysis.
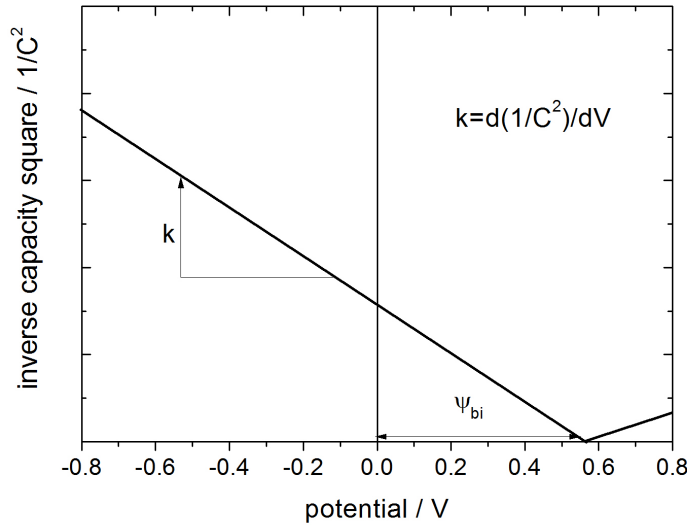
Figure 1.1.3:   Plot of $1/C^2$ vs. potential from impedance measurement. Schematic Mott Schottky analysis: the slope k indicated in the graph is proportional to the charge carrier concentration N_A. The built-in potential ψ_{bi} is determined directly from the intersection at y=0 with the x-axis. The depletion width ω is calculated from N_A and ψ_{bi}.

The total space charge Q_{SC} in the semiconductor is given by

$$Q_{SC} = \rho\omega = qN_A\omega = \sqrt{2q\varepsilon_S N_A\left(\Psi_{bi} - V_{applied} - \frac{kT}{q}\right)} \tag{1.1.12}$$

Therefore the capacitance is

$$C = \frac{dQ_{SC}}{dV} = \sqrt{\frac{q \cdot \varepsilon_S \cdot \varepsilon_0 \cdot N_A \cdot A^2}{(\Psi_{bi} - V_{applied}) \cdot 2}} \qquad (1.1.13)$$

For the capacity C per area A we obtain

$$\frac{C}{A} = C_A = \sqrt{\frac{q \cdot \varepsilon_S \cdot \varepsilon_0 \cdot N_A}{(\Psi_{bi} - V_{applied}) \cdot 2}} \qquad (1.1.14)$$

$$\frac{1}{C_A^2} = \frac{(\Psi_{bi} - V_{applied}) \cdot 2}{q \cdot \varepsilon_S \cdot \varepsilon_0 \cdot N_A} \qquad (1.1.15)$$

With derivation of equation 1.1.15 one gets the slope of the linear regime which is proportional to the charge carrier concentration and can be determined from the Mott-Schottky plot (figure 1.1.3).

$$k = \frac{d\frac{1}{C_A^2}}{d\Psi} = \frac{-2}{q \cdot \varepsilon_S \cdot \varepsilon_0 \cdot N_A} \qquad (1.1.16)$$

$$N_A = \frac{-2}{q \cdot \varepsilon_S \cdot \varepsilon_0 \cdot k} \qquad (1.1.17)$$

For a constant charge carrier concentration the slope intersects with the x-axis at y=0. The intersection is determined as the built-in potential ψ_{bi} [23, 24].

1.2 Organic Schottky diodes

MS-contacts are utilized for a variety of devices such as photo detectors or solar cells [23, 20, 22]. In comparison to usual pn-diodes, Schottky diodes offer a wide range of applications with an easy device geometry, a low forward-voltage drop and as a result a fast switching action between conducting and non-conducting mode. The formation of a Schottky barrier between an organic semiconductor and different metals has already been demonstrated by several groups. Kuo et al. [13] give account about Schottky diodes using poly-(3-hexylthiophene) (P3HT), doped with $FeCl_3$, as semiconductor and indium as blocking contact. G. Dennler et al. [4] report about the use of organic semiconductor Schottky contacts to investigate unusual electromechanical effects in organic materials due to piezoelectricity and electrostriction. Therefore they applied P3HT as organic semiconductor and doped it with oxygen by air exposure. They investigated an increase of capacity with time as a result for ongoing doping procedure. Figure 1.2.1 exhibits Mott Schottky analysis of the oxygen doped device, recorded successively every 2 min at 1 kHz in air.
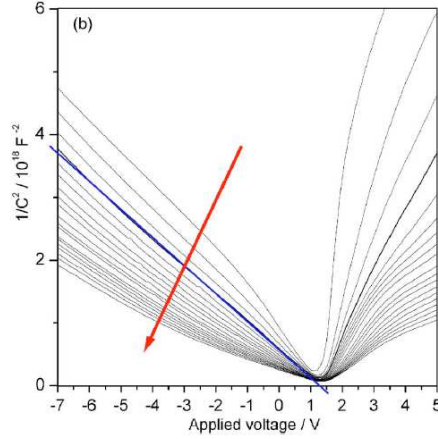
Figure 1.2.1: $1/C^2$ versus voltage V plot (measurement every 2 min at 1 kHz) of an ITO/P3HT/Al diode. Time increase is equivalent to the arrow direction. The blue line is a linear fit of one of the curves [4].

The groups of Bisquert and Garcia-Belmonte depict Schottky junctions of P3HT:PCBM blends and aluminum [1] [7]. In one work they investigate Schottky junctions between oxygen p-doped P3HT in a blend of P3HT:PCBM with capacity measurements. In another work they observed charge carrier recombination and diffusion in P3HT:PCBM/Al Schottky contacts by impedance spectroscopy. In figure 1.2.2 the Mott Schottky plot for this P3HT:PCBM/Al device is presented.
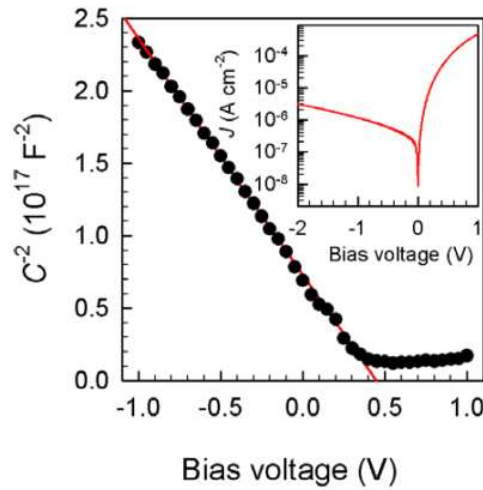
Figure 1.2.2:   Mott Schottky analysis yields built in potential $\Phi_{bi} = 0.43$ and charge carrier concentration $N_A = 3.10^{16}$ cm^{-3}. Inset: current density-voltage characteristics in the dark [7].

As already mentioned a certain doping concentration respectively charge carrier concentration is necessary for a Schottky barrier.

In a semiconductor like silicon free carriers are generated due to dopants, impurities at some positions of the lattice. These impurity atoms either possess more or less valence electrons than the silicon atoms itself. In case of dopants possessing more valence electrons than the main molecules, more unbound negative charges are available. Therefore such semiconductors are called n-type, n for negative. Are there dopants with less valence electrons, unbound positive charges are the majority charge carriers. These semiconductors are called p-type, p for positive. Majority charge carriers are electrons in n-type semiconductors and holes in p-type semiconductors. In a Schottky barrier mainly majority carriers are responsible for current transport, in contrast to p-n junctions where current transport is due to minority carriers.

In Schottky barriers with a n-type semiconductor, electrons move from the semiconductor to the metal. In case of a p- type semiconductor free holes can move across the interface [9]. In both cases the majority carriers are depleted from the semiconductor in the region near to the interface. A Schottky-blocking layer (depletion layer) is built, which is shown on the right hand side of figure 1.1.2 and in figure 1.2.5b, and has already been discussed in section 1.1.

If organic semiconductor materials are processed properly and appear in their pure form, they are intrinsic and require physical defects or chemical dopants to produce free carriers. Applicable polymers and other organic materials consist of conjugated double bonds, instead of a lattice like silicon. For organic semiconductors the doping principle is different. There are four main methods to achieve doping, as it is imaged in figure 1.2.3 for conjugated polymers.
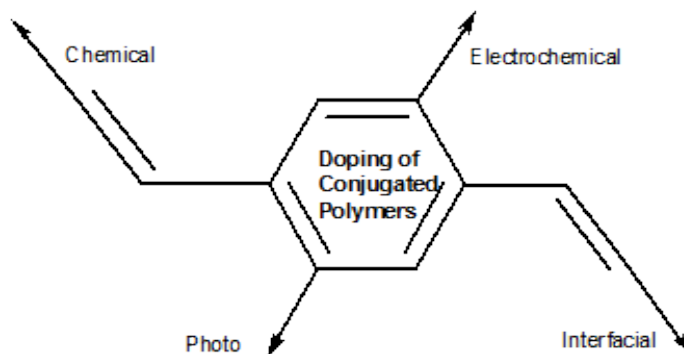
Figure 1.2.3: Doping methods of conjugated polymers. Figure courtesy of Heeger et al. [10].

For this study two of those doping methods were used. The first one is chemical doping and the second one is photo-doping. Photo-doping appeared as a side effect in our work through illumination during investigations of photovoltaic effects [8], presented and discussed in current-voltage characteristics in point 3.3.

If an organic semiconductor is illuminated at a certain energy, an electron is excited from the filled π-band to the empty π^*-band. This process can be regarded as a local oxidation at one place and local reduction at a different place of the conjugated backbone, depicted in following chemical reaction .

$$(\pi\text{-polymer})_n + h\nu \rightarrow [\{\pi\text{-polymer}\}^{y+} + \{\pi\text{-polymer}\}^{y-}]_n$$

Y is the number of electron-hole pairs which will form, due to Coulomb attraction, excitons- a neutral bond state .

Chemical doping means to be an oxidation or reduction. Since we focused on chemical doping by gas phase, discussed in section 2.1.3 this doping method will be explained more detailed too.

In contrast to doping of inorganic semiconductors doping of organic semiconductors is reversible and does not disturb the structure. Oxidation removes some π-electrons of the organic molecule. The organic semiconductor is oxidized and a positive carrier is free to move along due to π-conjugation (Figure 1.2.4). The dopant is reduced and a counter-ion, a localized negative charge, is inserted into the structure. The counter ion is able to move in and out of the structure and compensates the mobile positive charge that was generated by oxidation of the semiconductor. This describes p-type doping of the organic semiconductor. For reduction it works the other way round: electrons are added, a negative carrier is free to move and a positive charged counter ion is inset, therefore this doping is called n-type.

8

Conjugated double bonds enable delocalized electrons to move along. In this study only p-type doping of the organic semiconductors will be discussed.
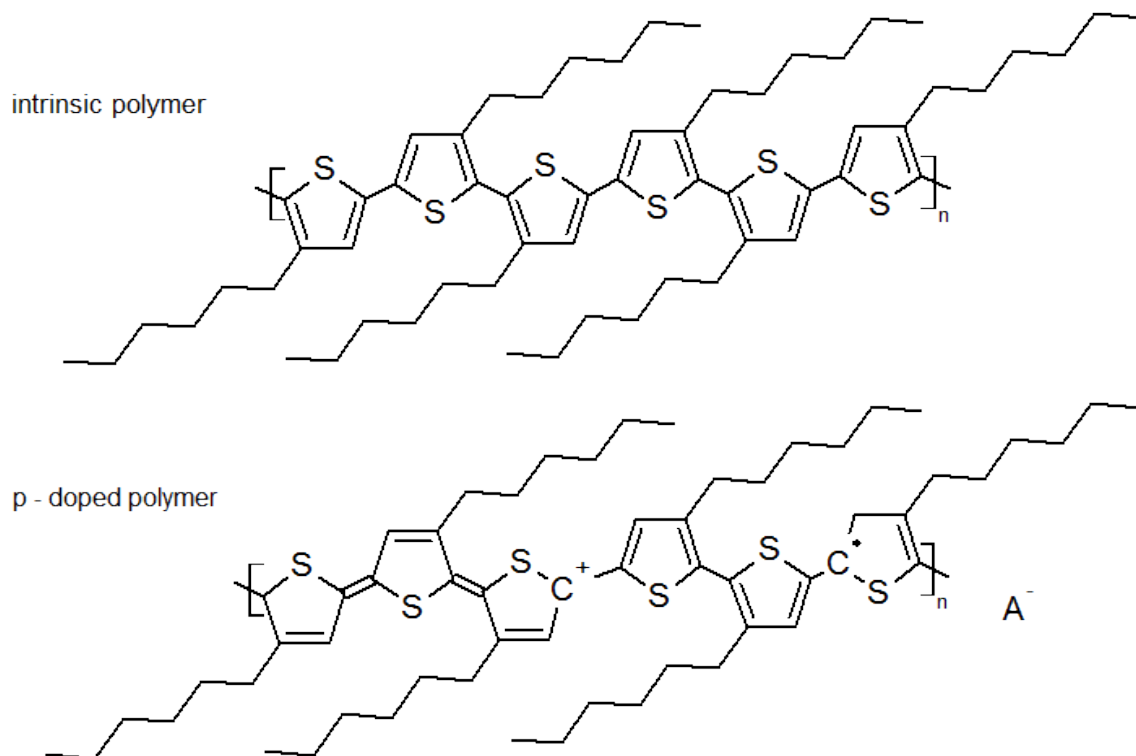
Figure 1.2.4:   Comparison of an intrinsic and a p-doped polymer. P- doped polymer: polaron generation in the polymer due to doping.

If an organic semiconductor, for example a polymer, is exposed to the vapor of a dopant such as iodine the doping is processed according the chemical reaction below.

$$3/2xy \ (I_2) + (CH)_x \rightarrow [(CH)^{y+}(I^{3-})_y]_x$$
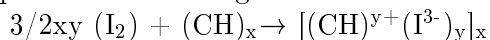
This reaction denotes p-type doping respectively oxidation of the polymer [10].

For Schottky barriers it is important to achieve a slightly doped semiconductor, which is the most challenging part for organic π-conjugated systems [18].

In the ideal case, without any thermal anomalies or surface states three states of doping can be regarded. Figure 1.2.5 illustrates the energy diagrams of a MS-interface with different doping concentrations of the p-type semiconductor.
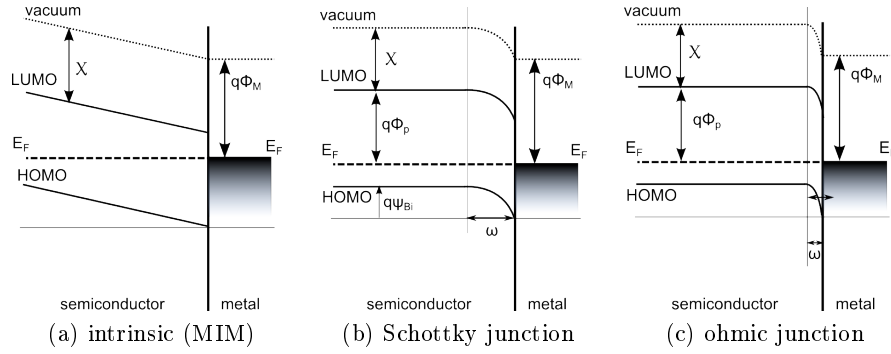
Figure 1.2.5:   Energy diagrams of a p-type semiconductor-metal system in different doping concentrations: a) intrinsic b) Schottky-type c) ohmic junction.

Figure 1.2.5a images the contact between metal and intrinsic polymer (MIM). There is no depletion layer formed and theoretically the width would exceed the film thickness (ω>d). Differently for a Schottky-type contact seen in figure 1.2.5b a voltage drop at the MS-contact is generated as already discussed for figure 1.1.2. A broad depletion width can be observed (ω<d) as a result for a slightly doped semiconductor. From the approximation of the valence band E_V of the semiconductor to the Fermi level of the metal, a distinct built-in potential ψ_{bi} can be determined. The last case represents a highly doped semiconductor. The depletion width is much smaller than the film thickness (ω<<d) describing an ohmic behavior (Figure 1.2.5c).

1.3 Characteristics of used materials

Organic Semiconductors

Applying organic semiconductors, especially polymers, has a few advantages. Organic materials are favored in handling and processability. Further organic semiconductors show advantageous properties, such as high stability, covalent bonds for charge transport, simple handling, mechanical flexibility and high availability. Due to those characteristics and in addition favorable properties in the visible range of light organic semiconductors like poly-(3-hexylthiophene) (P3HT), poly-[2-methoxy-5-(3', 7'-dimethyloctyl)-p-phenylene vinylene] (MDMO-PPV) and zinc phtalocyanine (ZnPc) have been used for solar cells and other applications. The group of Moet et al. [16] report about the application of MDMO-PPV and P3HT in hybrid solar cells with zinc oxide. They compared absorption properties of both polymers upon adding diethylzinc. Dennler et al. [5] investigated electromechanical effect in P3HT/Al Schottky diodes (see also section 1.2). Brabec et al. [2] investigated among others the behavior of zinc-phtalocyanine (ZnPc)/N, N M'-dimethylperylene-3,4,9,10-tetracaboxalic diimid (MPP) bilayer devices, aiming at enhancement of photovoltaic properties.

For this study P3HT, MDMO-PPV and ZnPc were applied for realizing a Schottky junction.

Figure 1.3.1:   Devices using different semiconductors. violet: P3HT, red-orange: MDMO-PPV, blue: ZnPc

Though all three materials belong to the group of organic semiconductors they possess different structures, including a polymer with a thiophene group, a polymer with a benzene group and a metal organic complex.

Semiconducting properties mainly come from delocalized electrons in the conjugation and valence bands that are formed by overlap of p_z orbitals [19]. As it is obvious from figure 1.3.2, figure 1.3.3 and figure 1.3.4 molecule structures of the chosen organic semiconductors meet all requirements for favorable semiconducting properties. P3HT consists of an aromatic heterocycle which contains conjugated double bonds as well as a sulfur atom, that provides, due to two free electron pairs enhanced charge delocalization (figure 1.3.2). In MDMO-PPV the conjugated double bonds of the benzene ring and the vinylene group are mainly responsible for moving of free charges (figure 1.3.3).
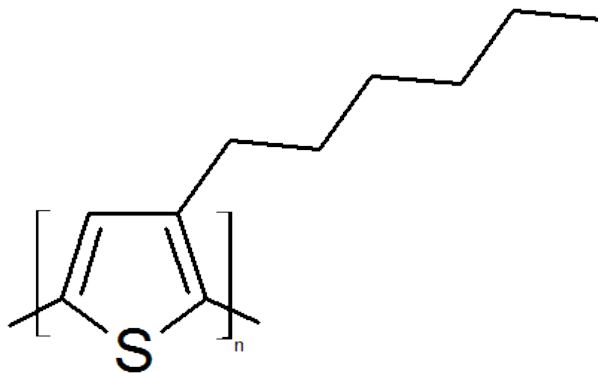
Figure 1.3.2:   Structure of P3HT poly-(3-hexylthiophene)
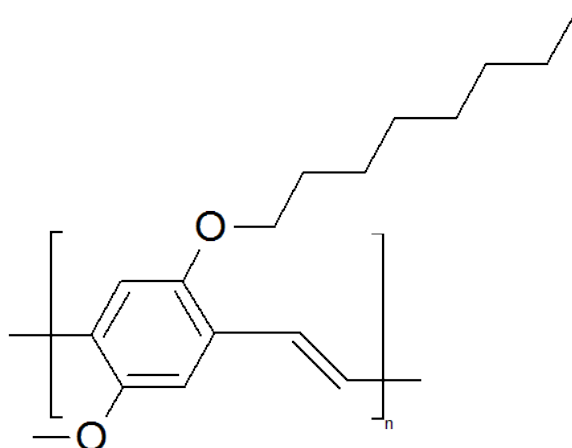
Figure 1.3.3:   Structure of MDMO-PPV poly-[2-methoxy-5-(3', 7'-dimethyloctyl)-p-phenylene vinylene]

ZnPc is a metal complex which shows a porphyrine similar molecular structure (figure 1.3.4). One zinc atom is surrounded by aromatic groups, which are advantageous for enhanced charge delocalization. The zinc atom in the middle of the complex and the surrounding nitrogen atoms share delocalized charges, which is also favorable for charge transport.
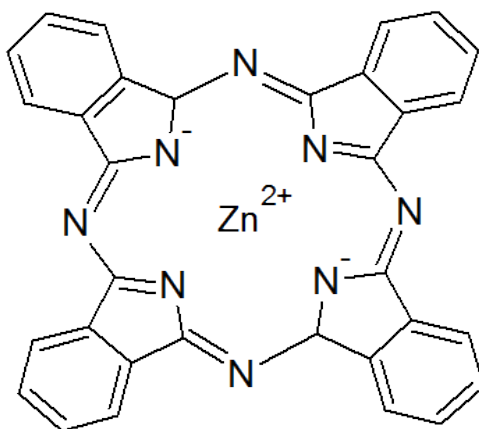
Figure 1.3.4:   Structure of ZnPc Zinc-Phtalocyanine complex

In figure 1.3.5a, figure 1.3.5b and figure 1.3.5c absorption properties of the three used organic semiconducting materials are presented. From their absorption features in the visible range of light the application of those materials for solar cells among others is obvious.
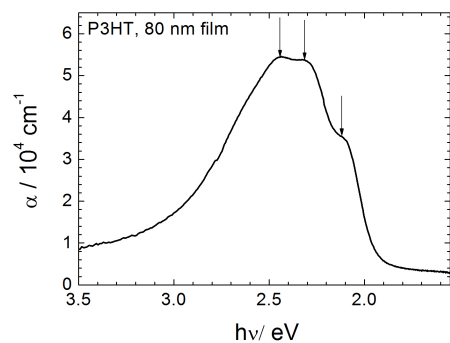
(a) Absorption of P3HT showing the distinct shape with maxima in the green regime of the visible range of light at 2.45, 2.29 and 2.12 eV
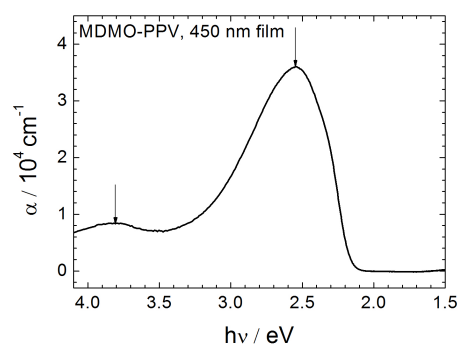
(b) Absorption of MDMO- PPV showing maxima in the green regime of the visible range of light at 3.84 and 2.54 eV
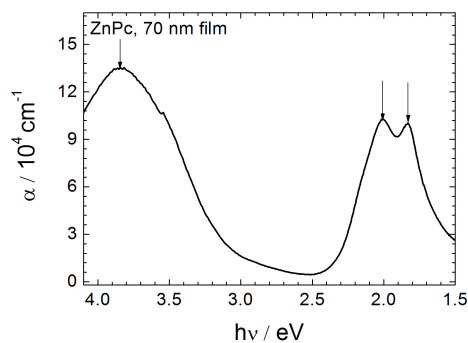
(c) Maxima of absorption of ZnPc in the blue regime of the visible range of light at 3.84 eV and in the red regime of visible light at 2.01 and 1.83 eV

Figure 1.3.5:   Absorption spectra of used organic semiconductors (P3HT, MDMO-PPV,ZnPc)

Doping

For chemical doping of organic semiconductors several substances are known. It has been published to use 2,3,5,6-tetrafluoro-7,7',8,8'-tetracyanoquinodimethane (F4-TCNQ) for molecular doping [14, 27]. The group of Ma et al. [14] investigated the relationship between electrical properties and the microstructure of P3HT when it is doped with the electron acceptor F4-TCNQ. Figure 1.3.6 shows their results on different doping states of P3HT in UV-Vis spectroscopy.
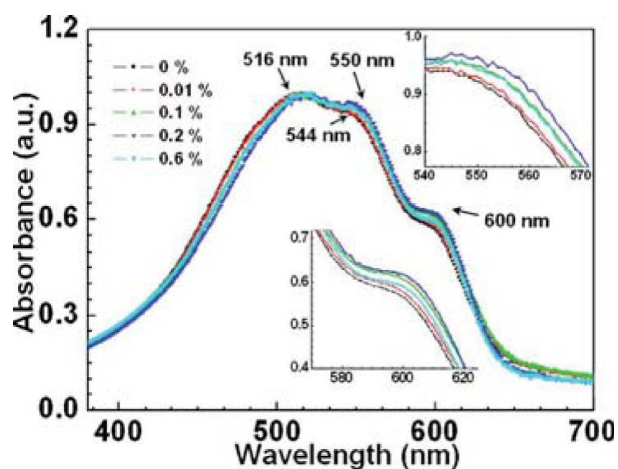
Figure 1.3.6:   UV-Vis absorption spectra of P3HT films with different F4-TCNQ concentrations. The insets show magnified images of the specified regions [14].

Zhang et al. depict results on controllable p-type doping of poly-[2-methoxy-5-(2'-ethylhexyloxy)-p-phenylene vinylene] (MEH-PPV) with F4-TCNQ [28]. Figure 1.3.7 presents current-density versus voltage characteristics of different dopant:host molar ratios.
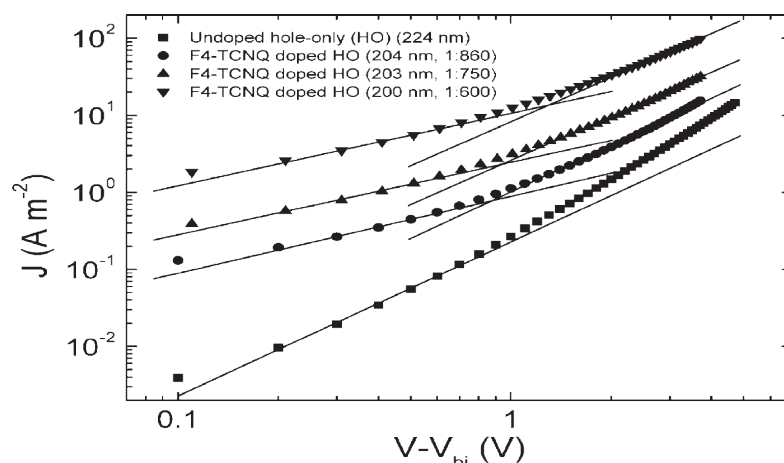
Figure 1.3.7:   Current-density vs. voltage characteristics of MEH-PPV HO devices for various dopant:host molar ratios. At low bias voltage the current density increases by 1-3 orders of magnitude with increasing doping concentration [28].

In another publication Zhang et al. report about controllable doping of P3HT with F4-TCNQ to investigate enhanced hole injection in P3HT/Ag Schottky diodes. Further they also investigated in this study conduction enhancement after doping of P3HT with iodine (see also section 1.2) [27].

As doping reagent for this study tridecafluoro-(1,1,2,2-tetrahydrooctyl)-trichlorosilane (FTS) was chosen. This organosilane shows favorable properties for more controlled doping respectively for slightly doping, which is necessary for Schottky junctions.

Figure 1.3.8:   Structure of tridecafluoro-(1,1,2,2-tetrahydrooctyl)-trichlorosilane

This material was used up to now for self assembled monolayers on substrates with hydroxide groups in a nucleophilic substitution reaction. Besides self assembled monolayers it has also been reported to apply FTS to organic semiconductor thin films as dopant.

Maddalena et al. [15] investigated kinetics of doping with FTS of P3HT using field effect transistors. They derived the dopant density as a function of exposure time and temperature. The groups of Podzorov et al. [11, 12] investigated the doping with FTS by exposing polythiophenes to FTS vapor. They claim that FTS incorporates deep into the nanoporous layer. The polymer chains are p-type doped by silanol groups of the hydrolyzed trichlorosilanes. The interaction of FTS with the polymers results in modification of optical properties and

increased electrical conductivity due to higher charge carrier concentration. Further they attempted to control the doping concentration in two different polymers. For their investigations they recorded absorption of different states in UV-Vis spectroscopy (figure 1.3.9). In a first step they measured the absorption of the polymer after spin coating and annealing. Afterwards the polymers were doped with FTS to saturation. Subsequently dedoping was recorded at different conditions (air atmosphere, time, dark or illumination with white light). Last the polymers were doped again.
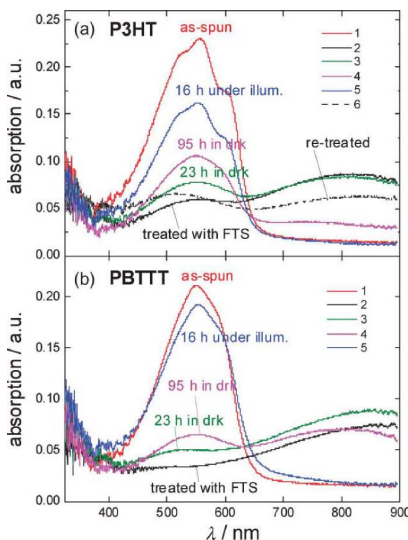
Figure 1.3.9: UV-Vis absorption of different doping states of P3HT and PBTTT with FTS. 1(red): as-spun annealed films, 2 (black): treated with FTS to saturation, 3 (green): dedoped in air in the dark for 23h, 4 (pink): dedoped in air in the dark for 95h, 5 (blue): dedoped in air under illumination with white light for 16h, 6 (dashed line): doped again with FTS after dedoping [11].

These results of Podzorov et al. are evidence of the controllability of FTS doping. For our studies we varied the time of vapor exposure for controlling the doping concentration. Still, the exact reaction during the doping process is unknown. We expect that during the doping process the alkyl silane is reduced at any position of the chain or maybe also at the silane group. Highly electronegative fluorine and chlorine atoms might act as electron acceptors and pull electrons from the organic semiconductor, that is subsequently oxidized.

Metals

Aluminum, samarium and magnesium/silver were used as metals respectively alloys for the top-contacts. These metals were chosen due to their low work functions (Table 2.1).

2 Experiments

2.1 Device Preparation

2.1.1 Choice of Substrate

For the study of photovoltaic effects in Schottky diodes, it was necessary to use transparent bottom electrodes. The material of choice was indium-tin-oxide (ITO), a transparent and conductive oxide. Therefore ITO covered glass was used. The ITO-glass was cut into 1.5x1.5 cm samples. To ensure later grounding of the top electrodes a stripe of 4 mm broadness was etched with concentrated hydrochloric acid (HCl, 37%) to remove the ITO.
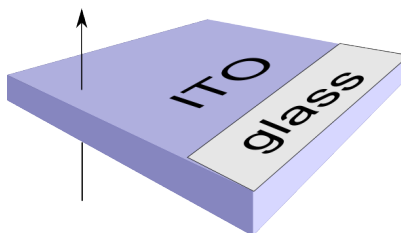
Figure 2.1.1:   Transparent bottom electrode on substrate: ITO on glass. A stripe of 4mm width of ITO is etched off for grounding of top electrodes

After that the sample substrates were cleaned by ultra sonic with acetone for about 20 min, subsequently with isopropanol for about 20 min and last with "base-piranha" solution (10 ml ammonium hydroxide NH_4OH in 200 ml 18.2 Ω water, heating at 80°C, adding of about 2 ml hydrogen peroxide H_2O_2).

2.1.2 Semiconductor layers

Spin coated semiconductors

The organic semiconductors P3HT and MDMO-PPV were purified first. Solutions of 20 mg of the polymer in 1 ml chlorobenzene C_6H_5Cl were prepared. After that each polymer was precipitated in Hexane C_6H_{14}. Centrifugation and vacuum drying delivered purified, solid polymers.

For spin coating solutions of 20 mg of the purified polymers per ml chlorobenzene were prepared. 40 µl of these solutions were put on the cleaned substrates. Subsequently spin coating was started with 2000 rounds per minute for 20 seconds and after that 3000 rpm for 10 seconds. Spin coating yielded a layer thickness of MDMO-PPV of about 450 nm (Figure

3.1.2) and of P3HT of about 80 nm (Figure 3.1.1). The polymer layers were annealed at 150°C for about 10 minutes.

To avoid oxygen doping, samples were stored in nitrogen atmosphere. Every step of work or measurement was performed in chambers of inert-gas atmosphere. Transfer between different workplaces was conducted with a special transfer chamber.

Thermally evaporated semiconductor

Zinc phtalocyanine was purified twice by temperature gradient sublimation. Evaporation was performed in UNIVEX thermal evaporation setup. The chamber was evacuated to a pressure of $3.8 \cdot 10^{-6}$ bar. The substrates were cooled with liquid nitrogen while the material was evaporated at a rate of 0.2-1 Å/sec. About 40 nm (Figure 3.1.3) of layer thickness were reached for Zinc phtalocyanine .

2.1.3 Doping

The doping process was performed by exposing semiconductor layers to the vapor of FTS. The time of exposure was varied referring to the layer thickness of the organic semiconductors. The exposure time of MDMO-PPV and P3HT was 7 minutes. Zinc phtalocyanine layers were exposed for 2 minutes. After that the polymer devices where annealed again at 150°C for about 5 minutes. Only the polymer diodes were annealed. A small stripe of the semiconductors was removed after doping for the ITO bottom contact.
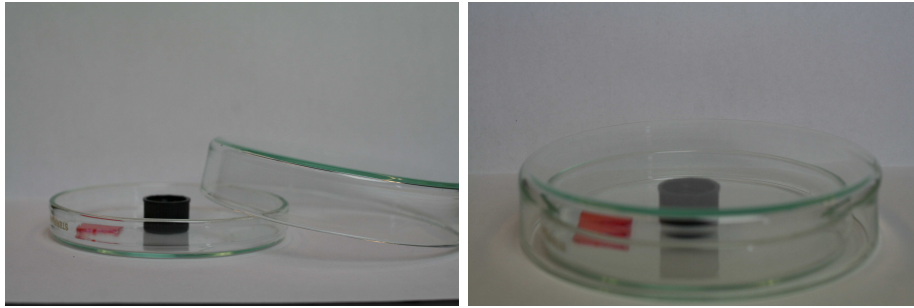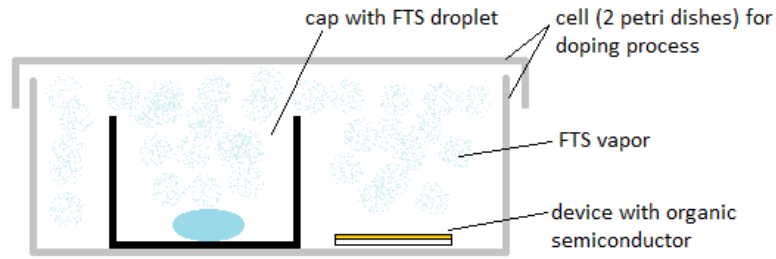
Figure 2.1.2:   Doping-setup: the first picture shows a schematic setup of the doping cell, on the left photograph below the cap containing a droplet of FTS in the open cell is shown; on the right photograph the closed setup for vapor exposition is presented.

2.1.4 Top- electrodes

In this study different metals were used to create Schottky barriers with the organic semiconductors (1.3, 2.1.2). The low workfunction materials aluminum, samarium and magnesium/silver (combined) were chosen. All metals were evaporated by thermal evaporation in vacuum (4-8$\cdot$10^{-6}bar) (table 2.1).

material	thickness d [nm]	workfunction [eV][23]
samarium	100	2.8
magnesium	90	3.7
silver	30	4.2
aluminum	100	4.3

Table 2.1:   Parameters for metal evaporation
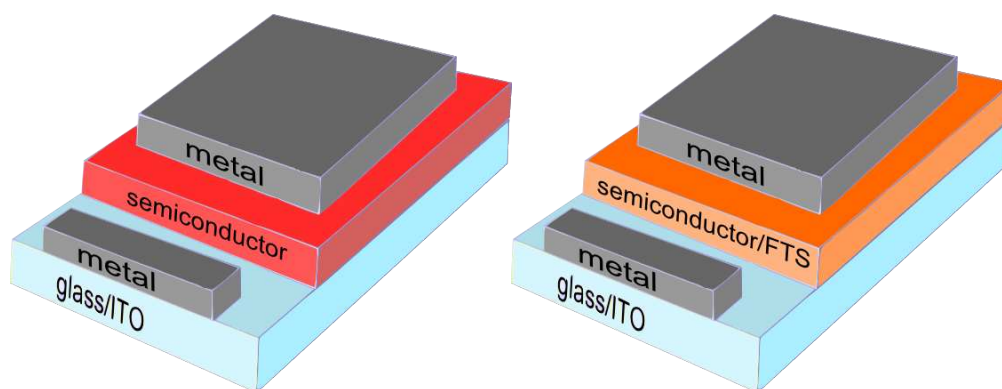
Figure 2.1.3:   Stack construction of intrinsic and doped devices: the left picture shows a device with an intrinsic polymer, the right picture shows the device after doping

2.2 Experimental Details

2.2.1 Atomic Force Microscopy

Atomic Force Microscopy was performed on MFP-3D-SA from Asylum Research, using a OMCL-AC240TS Cantilever from Olympus. Layer thickness and surface characteristics of the semiconductors were determined.

2.2.2 UV-Vis Measurement

Absorbance properties were measured in UV Vis-Setup Cary 3G UV-Visible Spectrophotometer to investigate the absorbance of doped and intrinsic semiconductors. The measurement was performed with thin films of the same thickness as usual devices for diode preparation. The effect of doping was inquired "ex-situ". After the doping the samples were measured.

2.2.3 Photoluminescence

Photoluminescence was measured at Horiba Jobin Yvon 670 measurement setup to verify the effect of doping with FTS. In case of ZnPc the doping was visible by change in color during the doping process. For P3HT and MDMO-PPV this effect was not observed (Figures 3.2.6 and 3.2.7). Photoluminescence measurement was used to achieve a deeper insight in the doping process of used polymers, which was performed ex situ in a standard doping setup (Figure 2.1.2).

2.2.4 Fourier transform infrared spectroscopy

Fourier transform infrared (FTIR) measurements were performed at Bruker IFS 66/S measurement setup for reliable in-situ monitoring of doping with FTS. The spectra were com-

pared to spectra of iodine doping. The absorbance of purified P3HT was compared to the absorbance of commercial P3HT.

2.2.5 Current-Voltage Characteristics

Current-voltage (I-V) measurements were performed in dark and light, to investigate in a first step diode like behavior and photovoltaic effect of the devices. Solar simulator (at AM 1.5) was used as a light source.

2.2.6 Impedance measurements

Impedance measurements were performed using an impedance analyzer HP 4284 A and the corresponding computer program of LabView. For the impedance measurements three different frequencies were chosen (300 Hz, 1 kHz, 1.5 kHz). The frequency was kept constant and the voltage was varied from -1.5 to 1.5 V for MDMO-PPV and from -0.8 to 0.8 for P3HT and ZnPc. The user interface of the program that was used for the impedance measurement is shown in figure 2.2.1. One is able to measure at constant frequencies and variable voltage, as it was done for this thesis, as well as at constant voltage and variable frequencies and variable voltage and variable frequency.
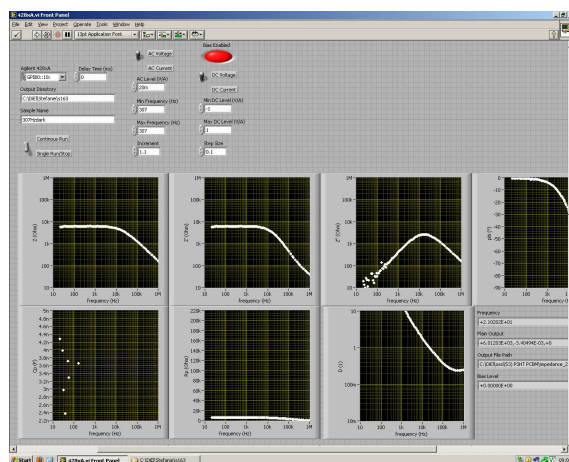
Figure 2.2.1:   Screenshot of the used program showing used parameters, such as frequency and voltage.

In addition the measurements were performed in dark and light. Depending on the maximum of absorption of the organic semiconductor (Figure 1.3.5a and 1.3.5c) a green LED (Golden Dragon 528 nm, 2 W) was used for P3HT and MDMO-PPV and the red counter-LED (Golden Dragon) was used for ZnPc.
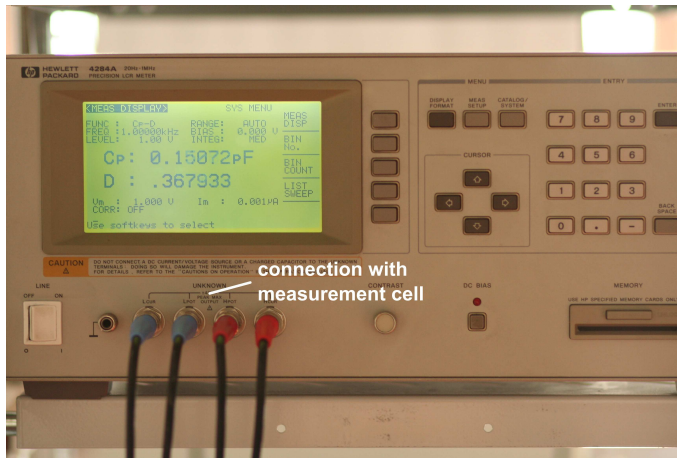
(a) Impedance analyzer HP 4284 A with connection to computer and measurement cell including the device
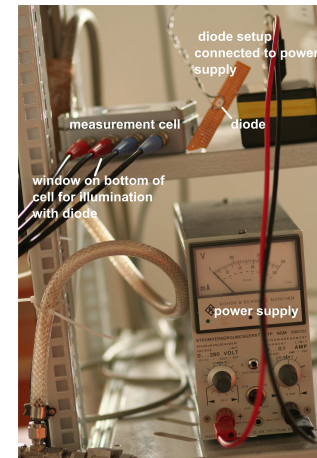
(b) Measurement cell including the device and diode setup for illumination of the cell, diode is switched on or off by the power supply
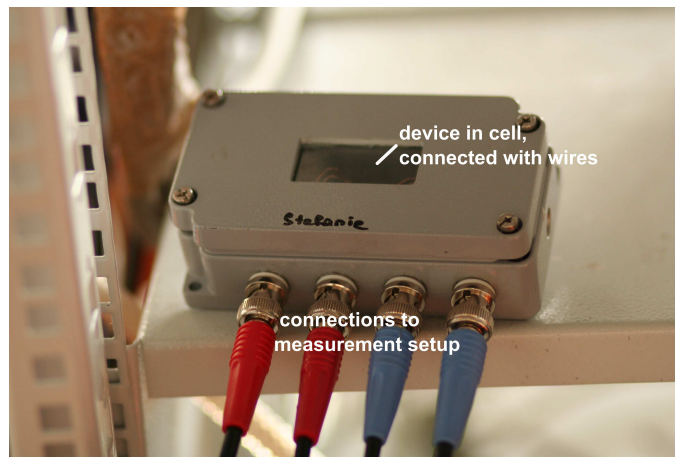
(c) Measurement cell with device inside, connected to the impedance analyzer

Figure 2.2.2:   Measurement setup for the impedance measurement with and without light

The results of the impedance measurements were investigated in Mott- Schottky analysis.

material	dielectric constant ε_s
P3HT	3.8[17]
MDMO-PPV	3[25]
ZnPc	3[26]

Table 2.2:   Permittivity of organic semiconductors

In table 2.2 the dielectric constants ε_s of the organic semiconductors are listed. Those values are necessary for the entire Mott-Schottky analysis and the contained calculations. Therefore ε_s is preferred in comparison to permittivity ε (C V^{-1}m^{-1}) because it is dimensionless.

3 Results

3.1 Nanomorphology

3.1.1 Atomic force microscopy

Investigation with AFM (atomic force microscope) shows layer thicknesses of P3HT of about 80 nm (Figure 3.1.1), of MDMO-PPV of about 450 nm (Figure 3.1.2) and of ZnPc of about 40 nm (Figure 3.1.3). Further rather smooth surfaces are observed for all organic materials.

For the layer thickness determination two measurement points were chosen: the first one on the organic semiconductor layer and the second one on the ITO, where the semiconductor was removed by a scratch. As a result for the scratching parallel lines are observed on the ITO for P3HT and ZnPc devices, because the semiconductors could not be removed completely. The measurement points are depicted as blue dots in the pictures on the left side as well as in the graphs on the right side . Pictures on the left feature the surface of the semiconducting layer respectively of the ITO and the transition between them obtained by a scratch. The right hand side graphs show the height of the layer versus the distance of measured points along the x-axis. The graphs of P3HT and ZnPc show both a maximum peak at 12 µm for P3HT respectively 18 µm for ZnPc. Those peaks are a result for the bulge of the semiconductor layer due to scratching.
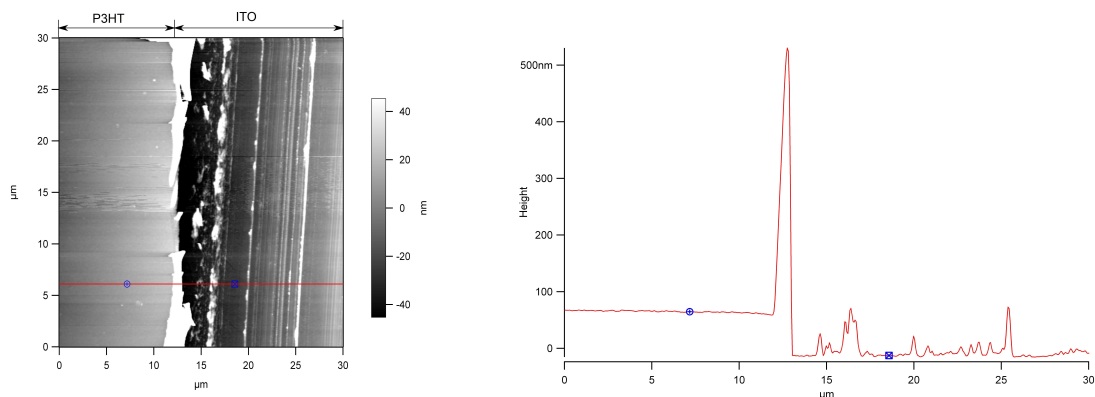
Figure 3.1.1:   AFM image (left side) and analysis of film thickness of P3HT/ITO transition (right side). The transition of semiconductor-ITO is shown after removing the semiconductor by a scratch.
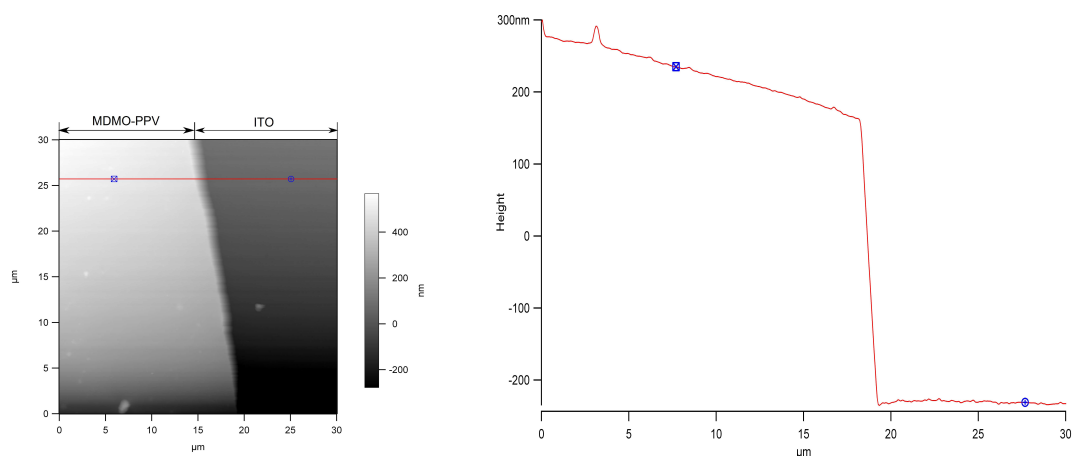
Figure 3.1.2: AFM image (left side) and analysis of film thickness of MDMO-PPV/ITO transition (right side). Smooth transition of semiconductor-ITO due to easy removable polymer.
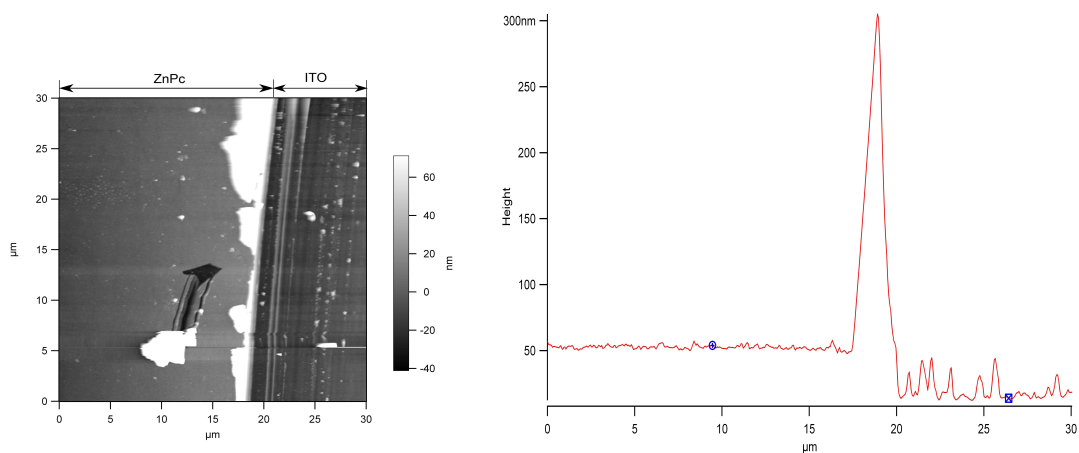
Figure 3.1.3: AFM image (left side) and analysis of film thickness of ZnPc/ITO transition (right side). The semiconductor was removed by a scratch from the ITO (defect in the semiconductor layer at y=10-15 µm due to scratching).

3.2 Spectroscopy

3.2.1 UV-Vis measurement

For comparison of absorbance of intrinsic devices to doped devices, UV-Vis spectroscopy was used.

As shown in figures 3.2.1, 3.2.2 and 3.2.3, absorbance features changed after doping procedure. The π-π* absorption was decreased in intensity after doping due to quenching.
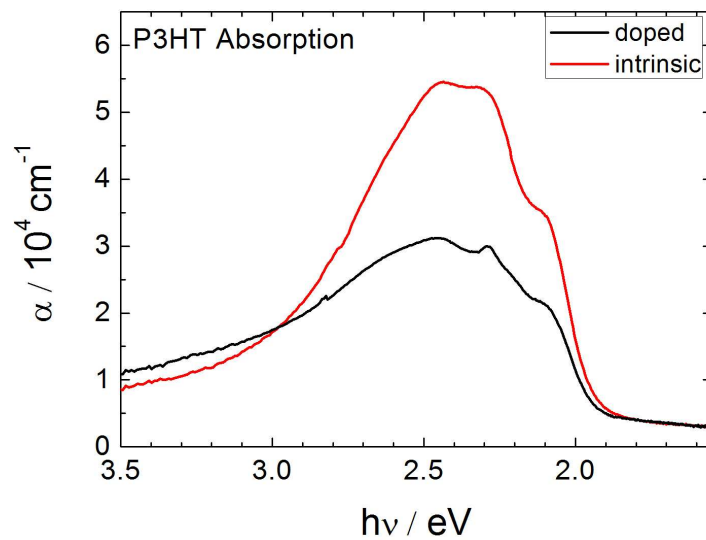
Figure 3.2.1:   Absorbance of intrinsic and doped P3HT as measured from a 80 nm thin film. Note the decreased absorption feature of the doped device.
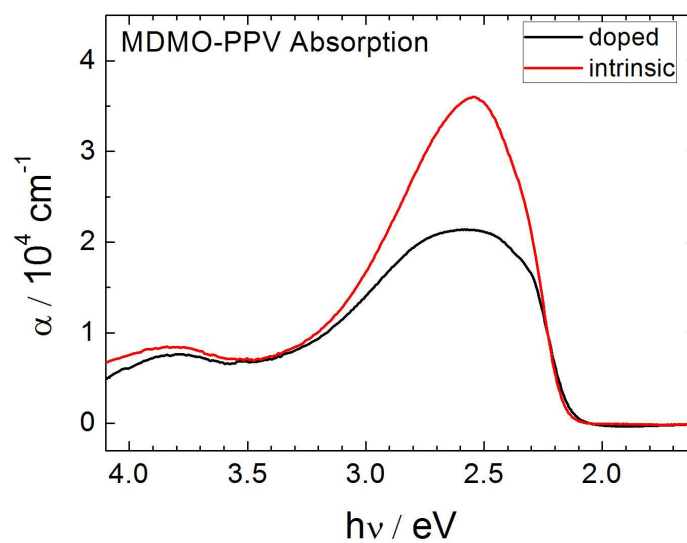
Figure 3.2.2:   Absorbance of intrinsic and doped MDMO-PPV as measured from a 450
nm thin film. The peak maximum is broadened through doping. Absorbance
decreased after doping.

The comparison of absorbance spectra of doped and intrinsic MDMO-PPV shows the same
effect as doping of P3HT. The intensity is decreased after doping. The peak maximum of a
doped device is broadened from 3.3-2.1 eV to 3.4-2 eV, compared to the feature of an intrinsic
device.
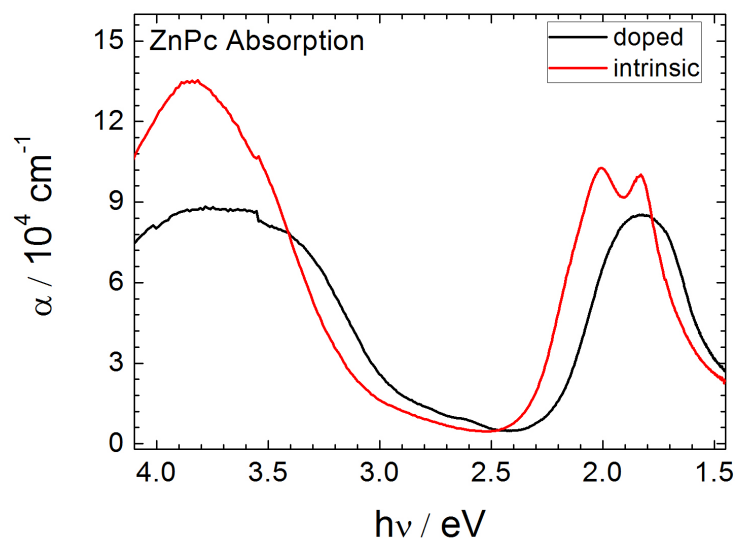
Figure 3.2.3:   Absorbance of intrinsic and doped ZnPc as measured from a 40 nm thin film. A distinct red shift and decreased absorbance after doping is shown.

The most influence of doping to absorbance properties shows ZnPc. The spectrum of a doped device shows an obvious shift to lower energies (red shift). Further the peaks of the Q band (2 eV and 1.8 eV) are merged together after doping. The signal between 4.1 and 3 eV decreased considerably.

The influence of FTS on absorbance properties was also investigated in IV-characteristics in photovoltaic investigations (3.3.1.1, 3.3.2.1, 3.3.3.1). Changes in photovoltaic behavior will be discussed in chapter 3.3.3.1.

3.2.2 Photoluminescence

As it is visible from Figure 3.2.6 and Figure 3.2.7 the emissions of the same thin films of P3HT and MDMO- PPV changed after doping. The intensities of the signals after doping are decreased distinctly. This effect is observed due to processes like excited state reactions or energy transfer that can be concluded as quenching. Figure 3.2.4 shows the decreased signals after doping of both polymers.

(a)

(b)
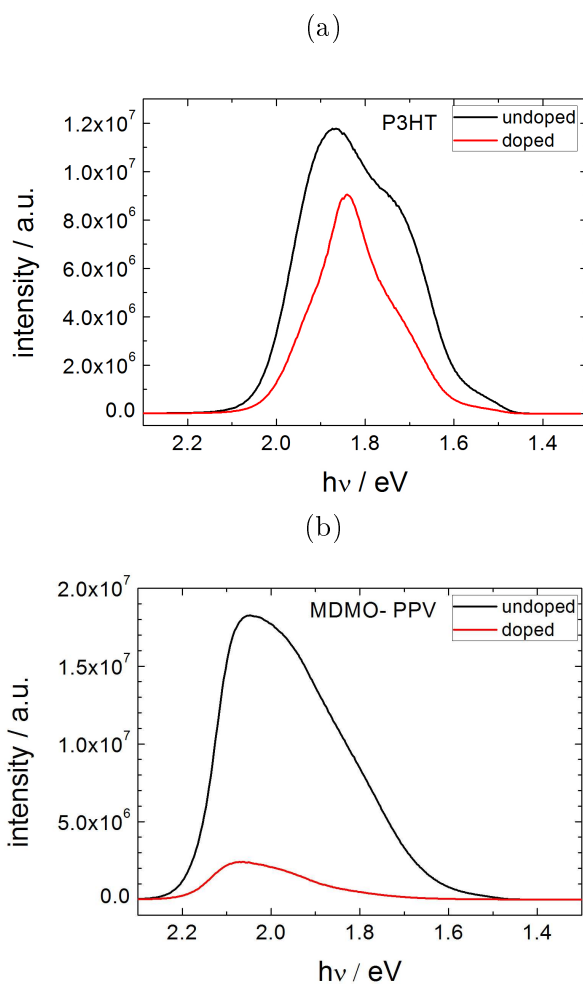
Figure 3.2.4: Photoluminescence spectra of P3HT (a) and MDMO-PPV (b) showing quenched signals after doping (red lines)

Compared to the emission spectrum of intrinsic P3HT, the emission spectrum of the doped polymer (figure 3.2.6) shows a narrower signal and the maximum of the signal is shifted to the right. The broad shoulder of the typical P3HT signal between 1.7 eV and 1.8 eV vanished. In MDMO-PPV the peak maximum is shifted to the left after doping (Figure 3.2.7). Further the signal shows a narrower emission range. The emission range decreased from 2.3-1.5 to 2.2-1.6 eV.

This results are observed due to counteracting of photoinduced electron transfer with photoluminescence. In a photoinduced electron transfer for a energetically favorable case a photon excites an electron from the π-band to the π^*-band, leaving a hole in the π-band. If the electron transfer is faster than the photoluminescence decay, electron and hole are separated. Energy is transferred nonradiatively. The doped material acts as an acceptor and the energy

of excitation is therefore bigger than the energy of the decay. As a result the intensity is quenched [10, 21].

These experiments result in the prediction that due to the quenching of the intensity of photoluminescence FTS treatment is doping.

The change of emission of ZnPc was not measured because the doping effect was visible as a change of the thin film color from blue to green as it is shown in figure 3.2.5.
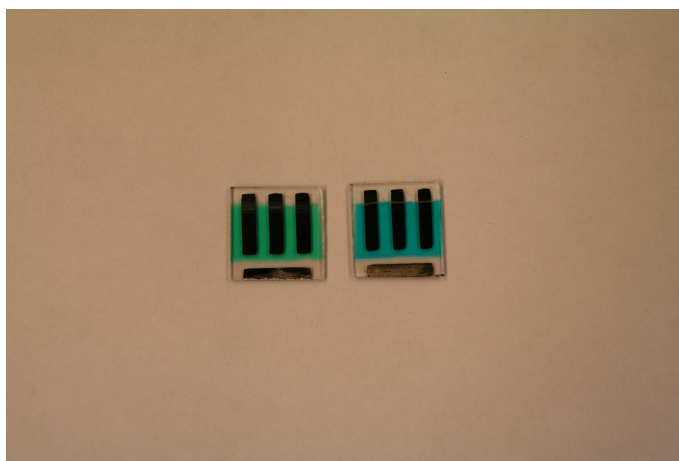
Figure 3.2.5:   Color change (change of emission) from blue (right side) to green (left side) of ZnPc thin films as a result of doping,
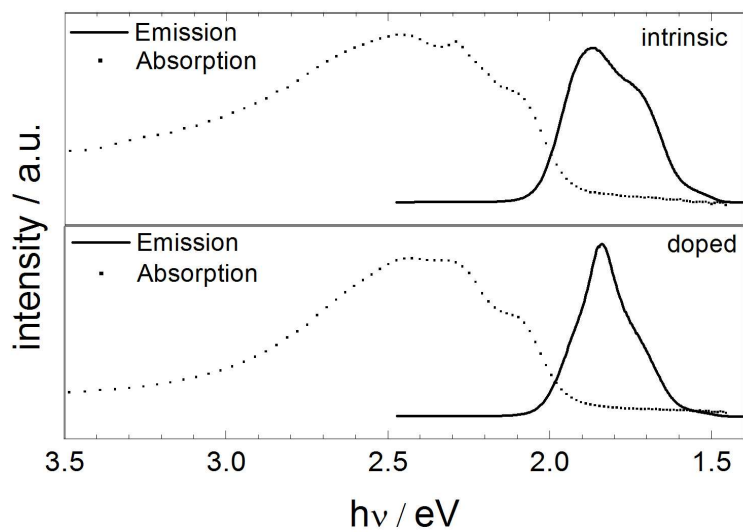
Figure 3.2.6: Photoluminescence of intrinsic and doped P3HT, the dashed lines show the shift between absorption and emission
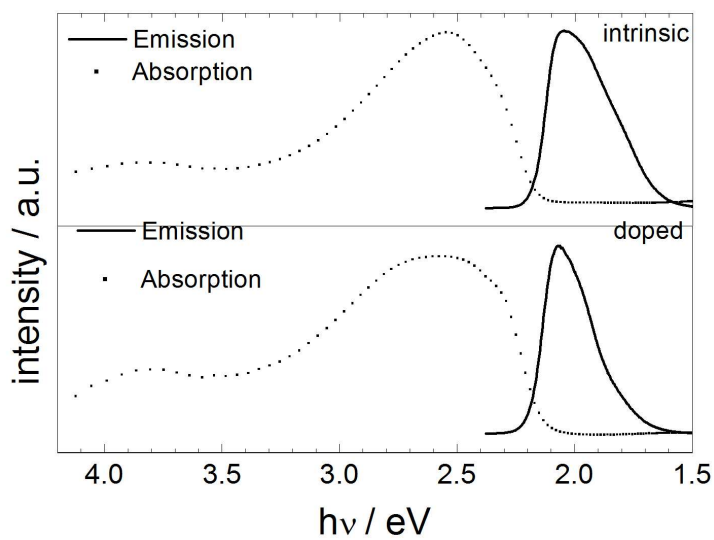
Figure 3.2.7: Photoluminescence of intrinsic and doped MDMO-PPV, the dashed lines show the shift between absorption and emission

3.2.3 Fourier transform infrared spectroscopy

To determine the absorption behavior of P3HT and FTS and further to investigate changes in absorption of purified P3HT and commercial P3HT infrared spectra of the materials were measured (Figures 3.2.8 and 3.2.9)

(a)

(b)
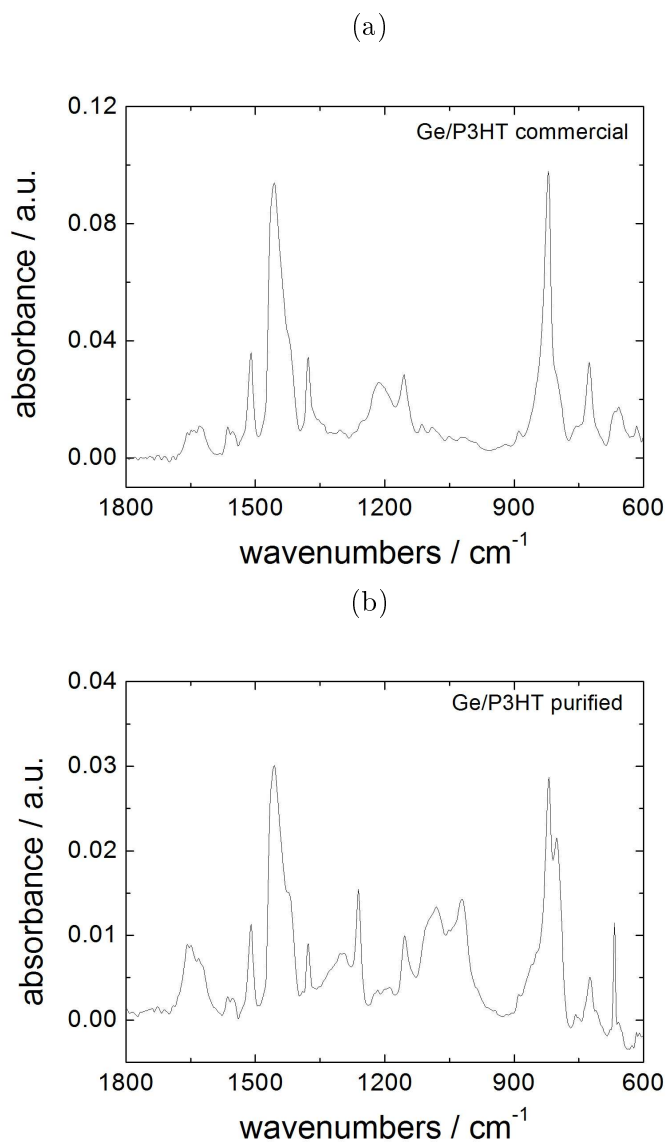
Figure 3.2.8:   Infrared spectra of commercial P3HT (a) and purified P3HT (b)
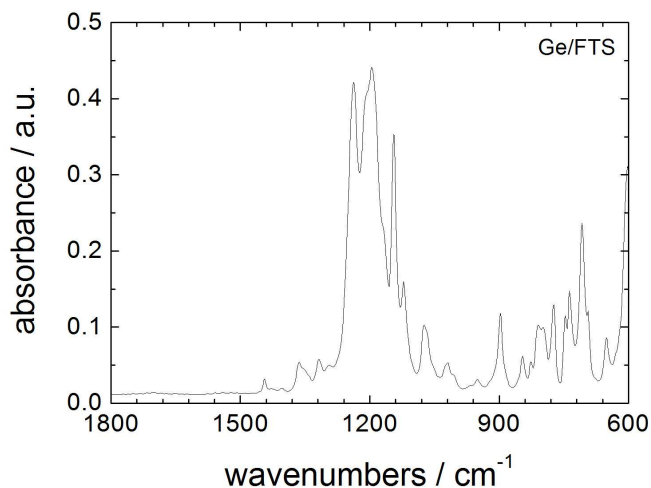
Figure 3.2.9:   Infrared spectrum of FTS

These spectra are used for identification of the IR spectra features.

From the FTIR experiments the doping behavior of FTS is observed as slow chemical doping compared to iodine doping, where the semiconductor is also exposed to vapor. Figure 3.2.10 shows the infrared spectra of FTS doping over 2 h of time. Every 5 min a new scan was started.

In figure 3.2.10 the important features like C=C vibrations and the $\delta(\text{C-H}_x)$ bending vibration between 1800 and 1400 cm^{-1} cannot be investigated more precise due to the interfering water signal over this range. At 670 cm^{-1} and 2350 cm^{-1} CO$_2$ signals from air interfere with the signals of the polymer. Below 1500 cm^{-1} fingerprint region is observed, which gives more details about the identity of the molecule and consists of sketching, bending and combination vibration bands. Below 1500 cm^{-1} C-F vibrations are apparent further. Through doping a dipole moment is induced. As a result IRAV (infrared active vibration) bands in the finger print region can be observed for polymers. Doping induced polarons are observed as polaronic feature between 5000 and 1500 cm^{-1}.

In figure 3.2.11 iodine doping process is imaged. The measurement was performed continuous, scans where started immediately.

In comparison to FTS, iodine dopes P3HT rather fast (Figure 3.2.11). Therefore FTS doping is easier to control. Spectra of Iodine and FTS doping show similar characteristics to be interpreted as evidence of doping: the distinct polaronic absorption between 1500 cm^{-1} and 5000 cm^{-1} and IRAV bands below 1500 cm^{-1}.

(a)
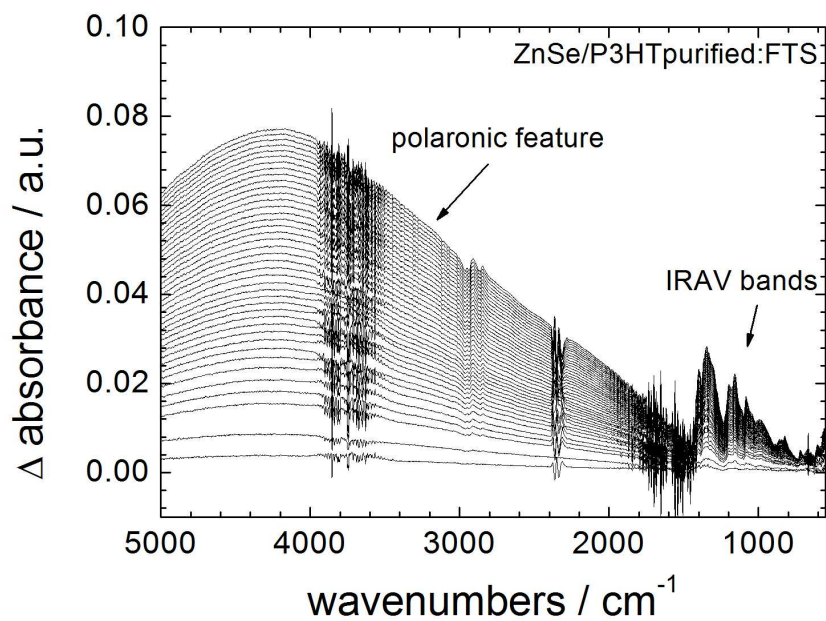
(b)
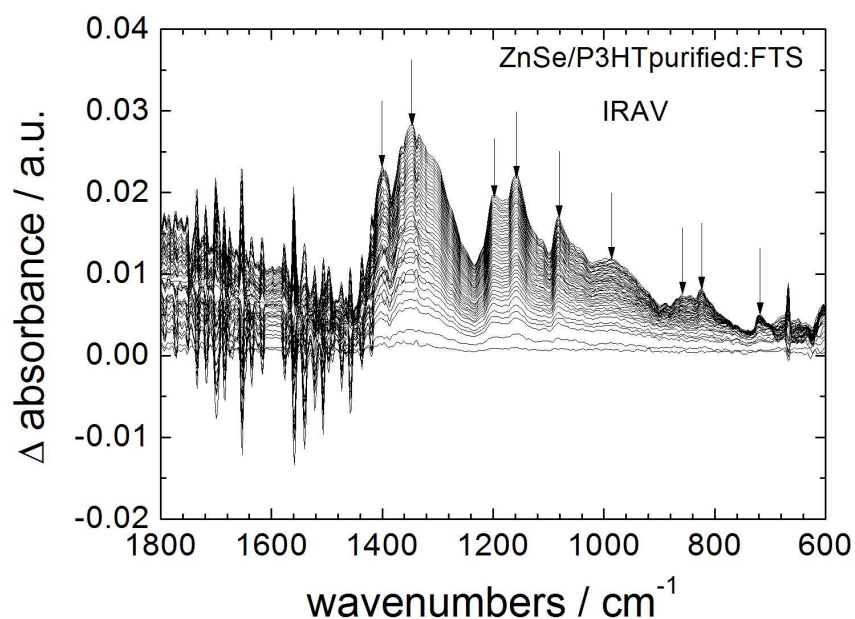
Figure 3.2.10: FTS doping of purified P3HT. 41 scans successively every 5 min; entire spectrum (a) and zoom of IRAV bands (b). Original IR spectrum was substracted from each consequent spectrum (delta absorbance). Additionally the H_2O and CO_2content was substracted in the regime of 3600-3900 cm^{-1}.

(a)
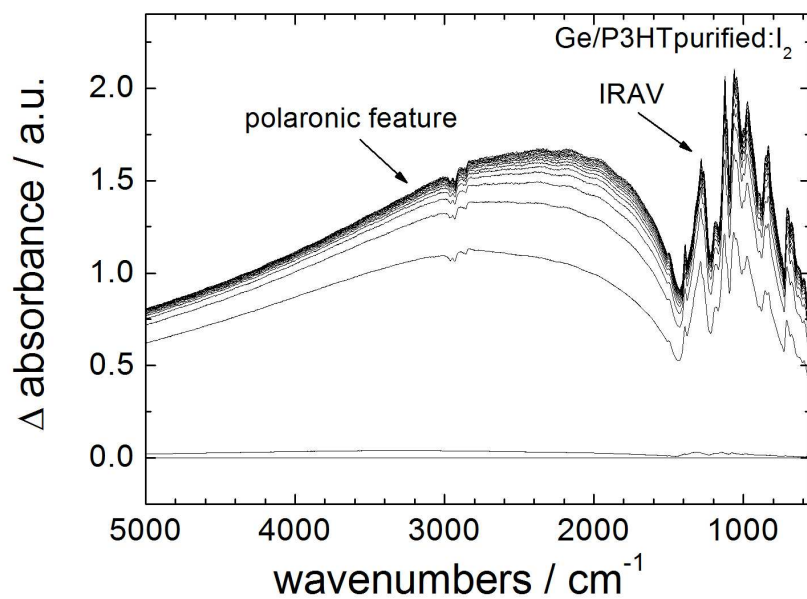
(b)
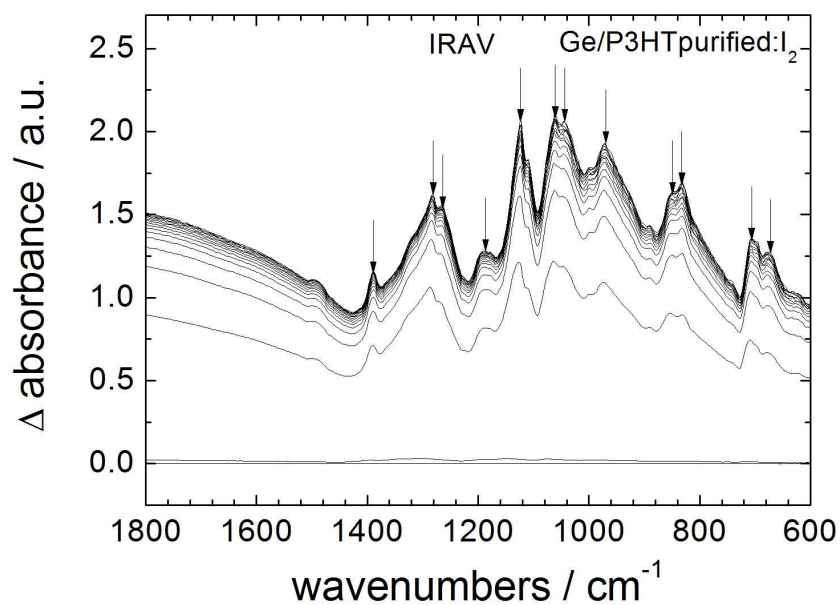
Figure 3.2.11:   Iodine (I$_2$) doping of purified P3HT. Continuous measurement (immediate start of next scan); entire spectrum (a) and zoom of IRAV bands (b). Original IR spectrum was substracted from each consequent spectrum (delta absorbance).

3.3 Characterization of Diodes

3.3.1 Poly-(3-hexylthiophene) devices

3.3.1.1 Current-Voltage Characteristics

The most promising results concerning P3HT-diodes with photovoltaic effect show devices with Al electrodes. Without illumination intrinsic P3HT devices do not behave like diodes. Illumination might induce charges, therefore the diode behavior is increased slightly.
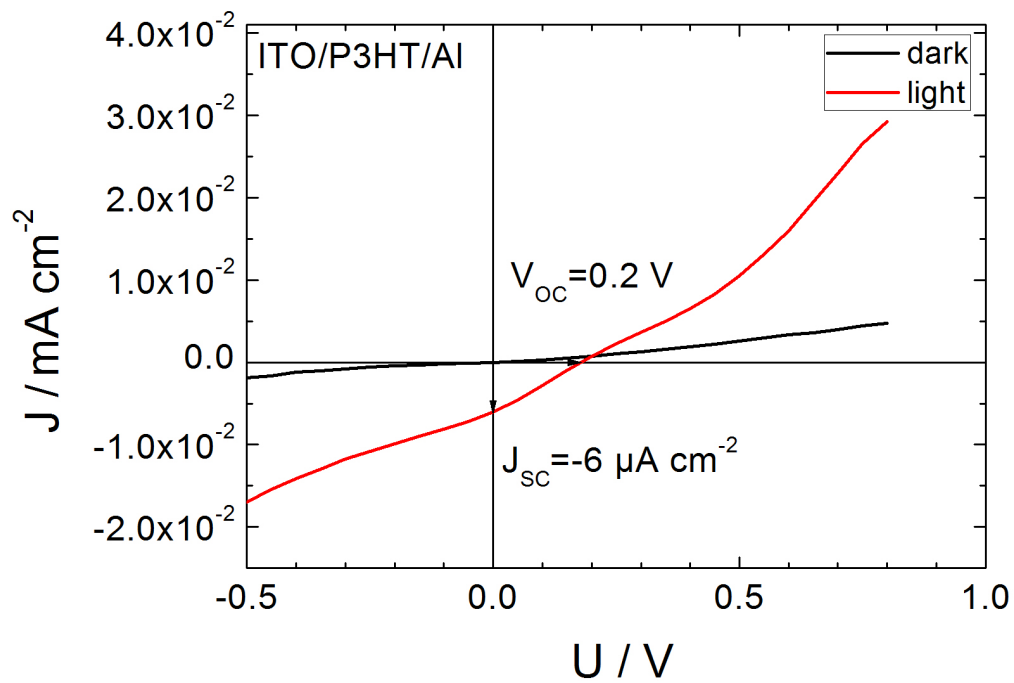
Figure 3.3.1:   Current density versus voltage, linear plot of an intrinsic P3HT/Al device
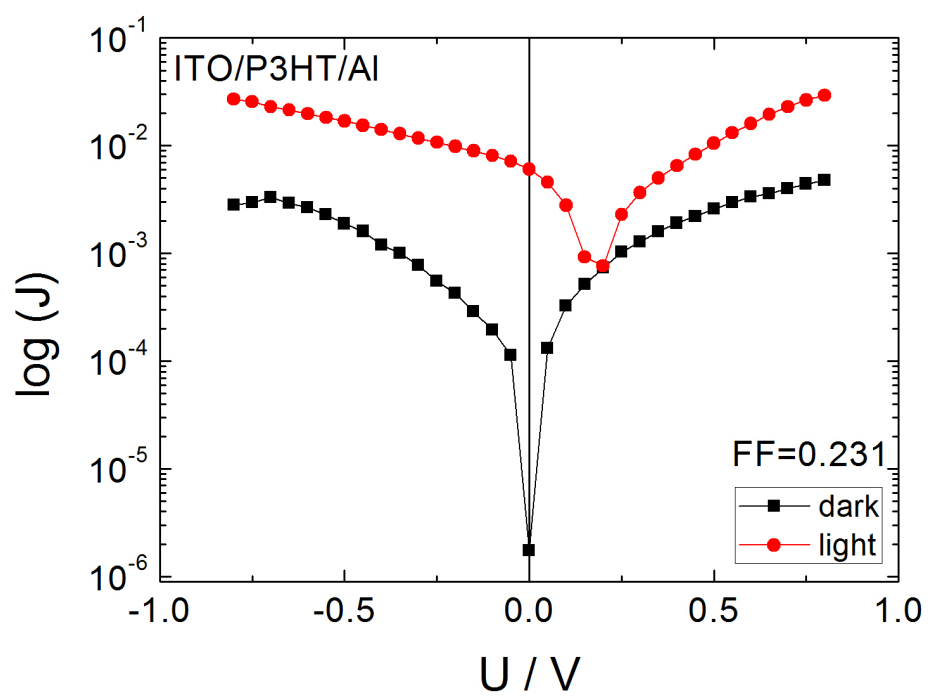
Figure 3.3.2:   Logarithmic plot of an intrinsic P3HT/Al device

If we compare figure 3.3.1 and figure 3.3.3 (Logarithmic plots: figure 3.3.2 and 3.3.4) it is obvious that doping with FTS improves the diode like behavior. However, the photovoltaic effect is reduced upon doping. The open circuit potential V_{OC} decreases from 0.2 to 0.1 V.
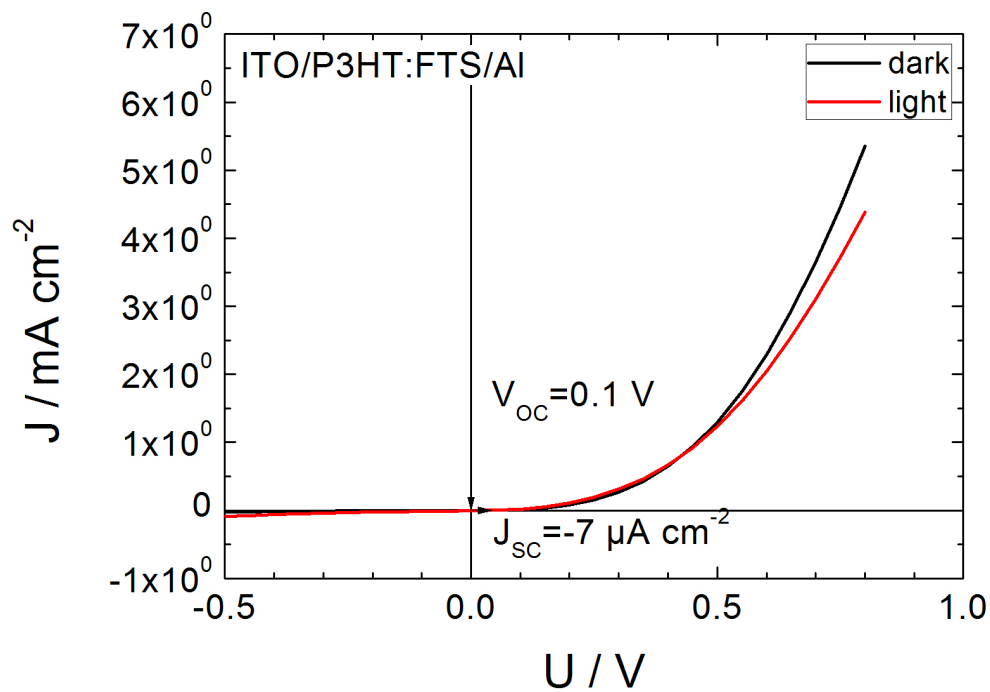
Figure 3.3.3:   Current density versus voltage, linear plot of a doped P3HT/Al device
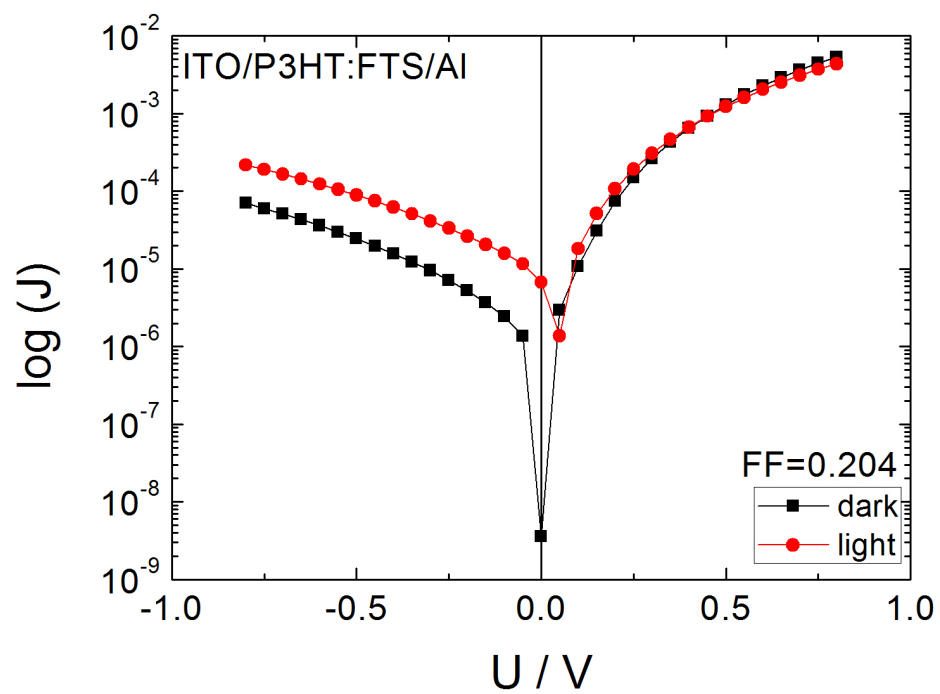
Figure 3.3.4:   Logarithmic plot of a doped P3HT/Al device

Again also for intrinsic P3HT/MgAg devices no distinct diode like behavior is observed. Even illumination does not improve rectification.

Figure 3.3.5:   Current density versus voltage, linear plot of an intrinsic P3HT/MgAg device
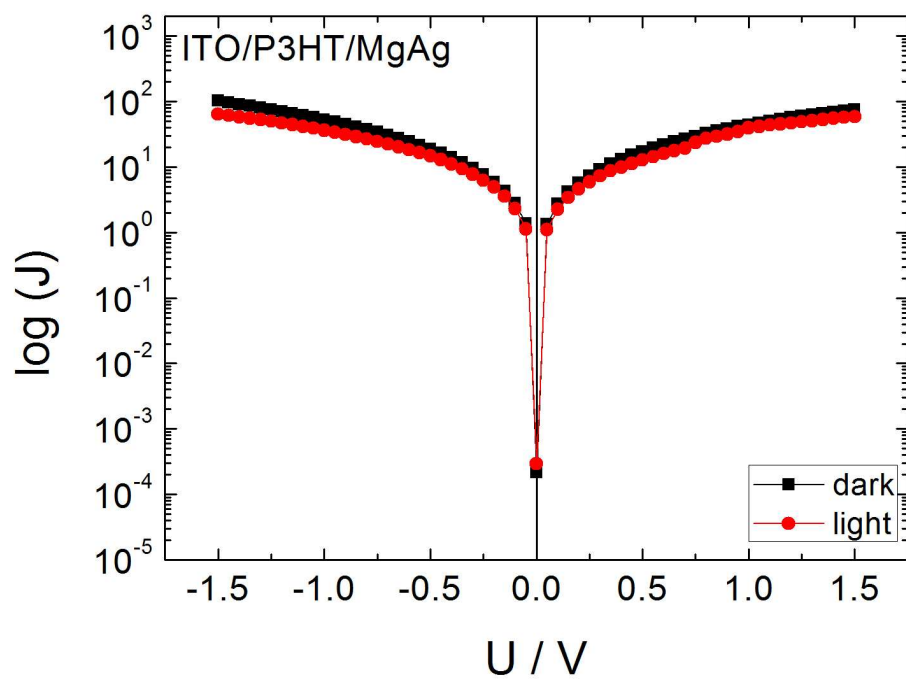
Figure 3.3.6:   Logarithmic plot of an intrinsic P3HT/MgAg device

Figure 3.3.5 and 3.3.6 and show the behavior of an intrinsic P3HT Diode. Due to missing free charge carriers V_{OC} and J_{SC} are zero.

Doped samples with Mg/Ag electrodes show good diode behavior and further, compared to devices with Al electrodes, a higher photovoltaic effect with high V_{OC} (Figures 3.3.7 and 3.3.8). Doping of the polymer increases V_{OC} to 0.4 V which is the highest value that could be achieved for P3HT diodes in this study.

Figure 3.3.7:   Current density versus voltage, linear plot of a doped P3HT/MgAg device
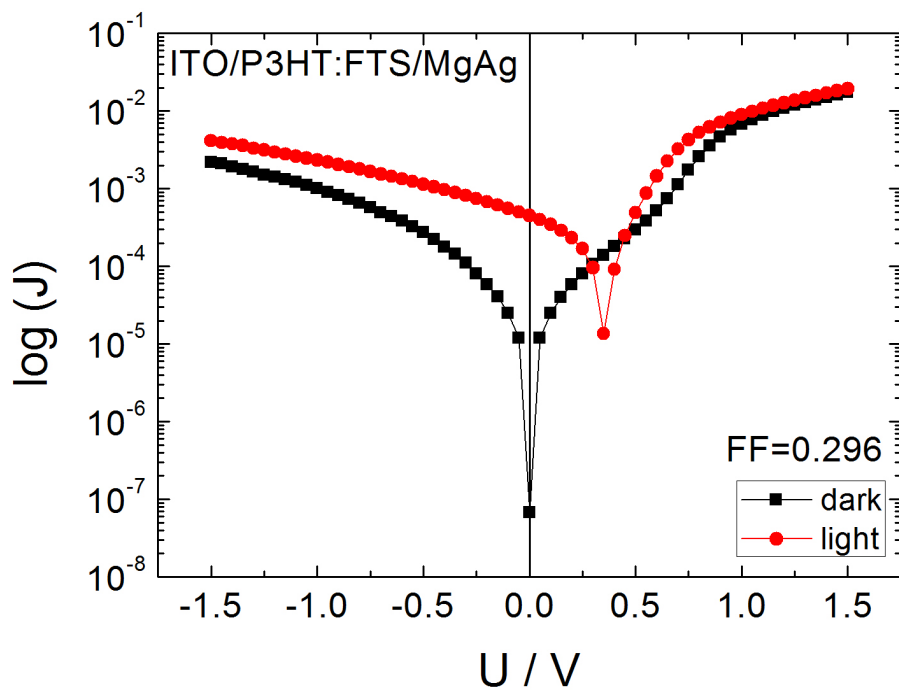
Figure 3.3.8:   Logarithmic plot of a doped P3HT/MgAg device

Applying samarium electrodes to P3HT devices is particularly challenging to fabricate. Intrinsic devices show short circuits. For doped devices just very little diode behavior is observed. Photovoltaic effects were neither observed in intrinsic nor doped devices. Samarium is a metal which is very sensitive to air moisture and oxygen because it is oxidized easily. Further P3HT is also very sensitive to oxidation. Therefore these circumstances constitute an obstacle for sufficient diodes and results are not presented in this work.

3.3.1.2 Mott Schottky Analysis

Impedance measurements of P3HT devices were just successful for samples with aluminum electrodes. Therefore Mott Schottky analysis was just performed for aluminum devices. The charge carrier concentrations were calculated using equation 1.1.17.
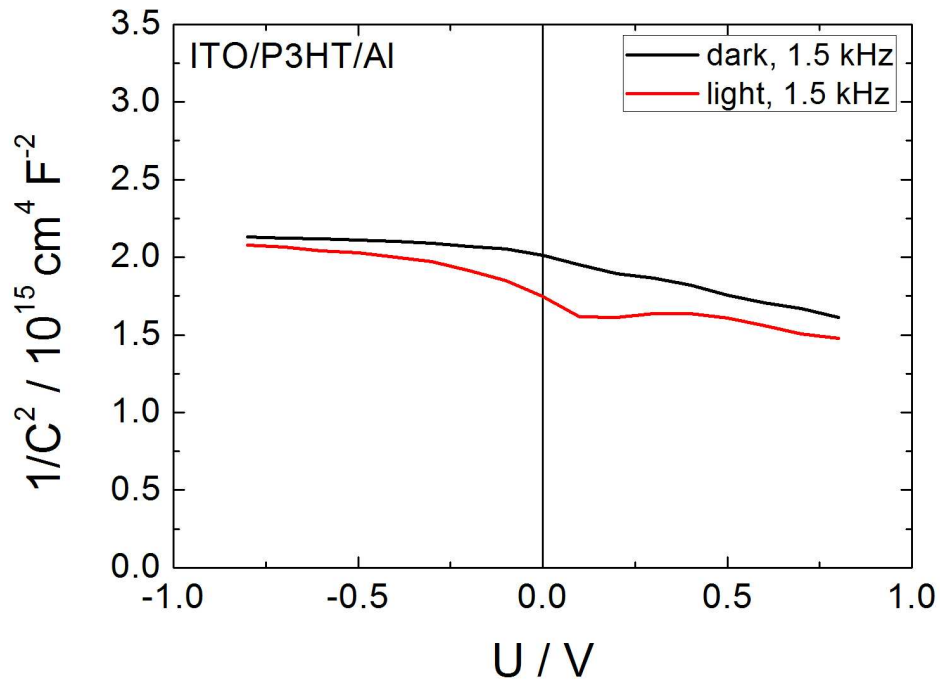
Figure 3.3.9: $1/C^2$ versus voltage plot of an intrinsic P3HT/Al device

The intrinsic device does not contain free charge carries and shows therefore no distinct linear regime. For that reason the charge carrier concentration could not be calculated (figure 3.3.9).
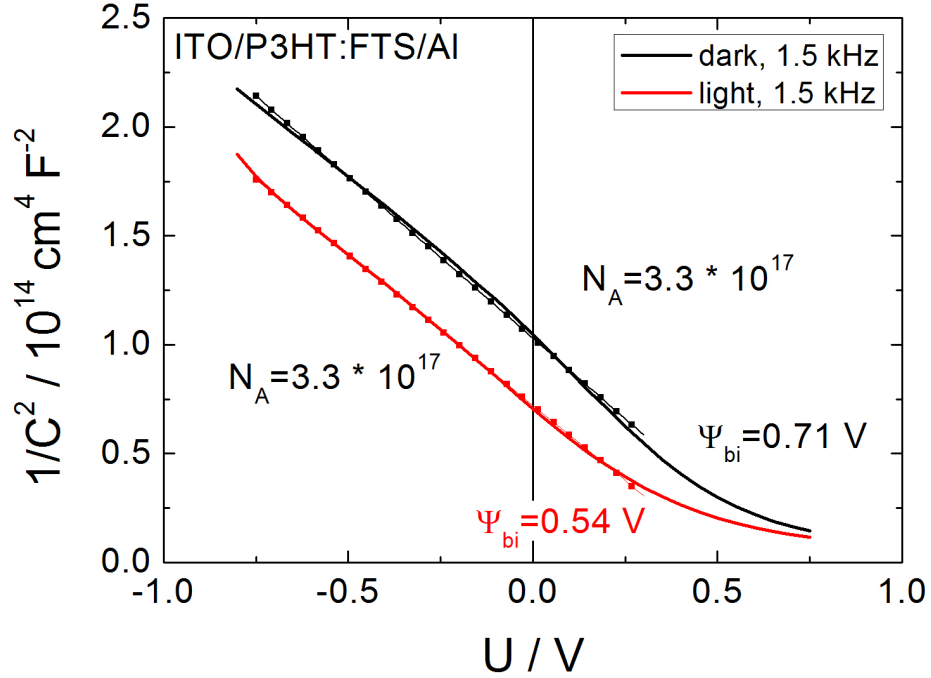
Figure 3.3.10: $1/C^2$ versus voltage plot of a doped P3HT/Al device

For the device that was doped with FTS, a carrier concentration of 10^{17} cm^{-3} could be determined. The intersection of the linear regime with the x-axis at y=0 characterizes a homogenous charge carrier concentration and enables determination of the built-in potential. The built-in potential in the dark is with a value of approximately 0.71 V higher than the built-in potential with light excitation, which is at 0.54 V. The depletion width at 0 V for the doped device is determined with formula 1.1.10. Without light excitation 31 nm of width were calculated and 29 nm for measurement under light.
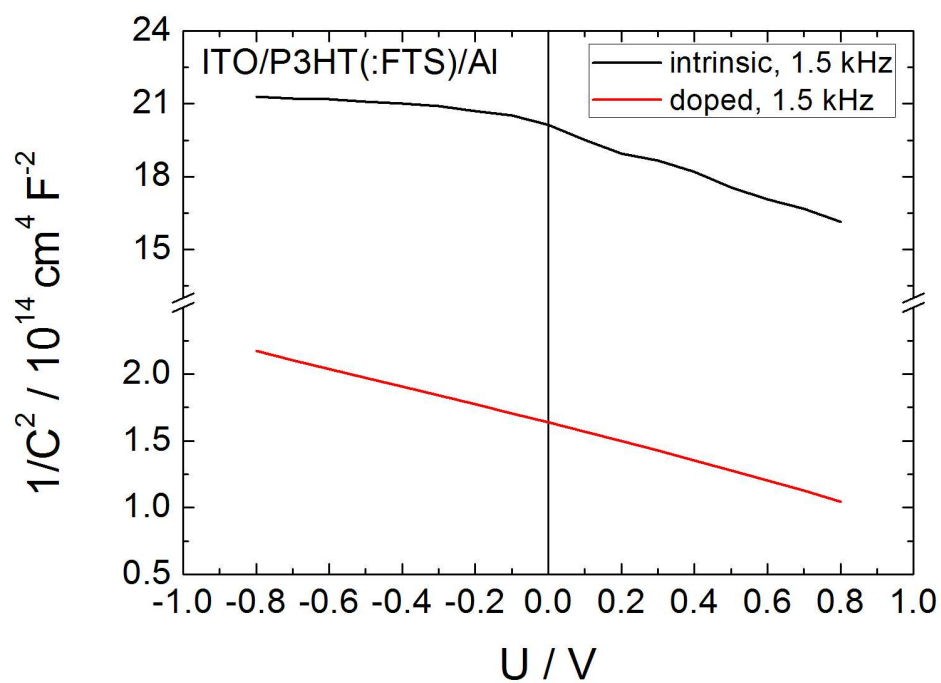
Figure 3.3.11:   Plots of $1/C^2$ vs. voltage of intrinsic and doped P3HT capped with Al are compared. For the doped device a linear regime is observed in contrast to the intrinsic device.

3.3.2 Poly-[2-methoxy-5-(3', 7'-dimethyloctyl)-p-phenylene-vinylene] devices

3.3.2.1 Current-Voltage Characteristics

MDMO-PPV devices show the best diodes among all experiments of this thesis. The devices have high open circuit potentials and fill factors in photovoltaic characterization, especially for top electrode-metals with low workfunctions, like samarium and magnesium/silver. Intrinsic devices of MDMO-PPV/MgAg depict rectification after illumination, which again (see also figure 3.3.1 and 3.3.2) might be due to photodoping, injection of charges by light (hν).
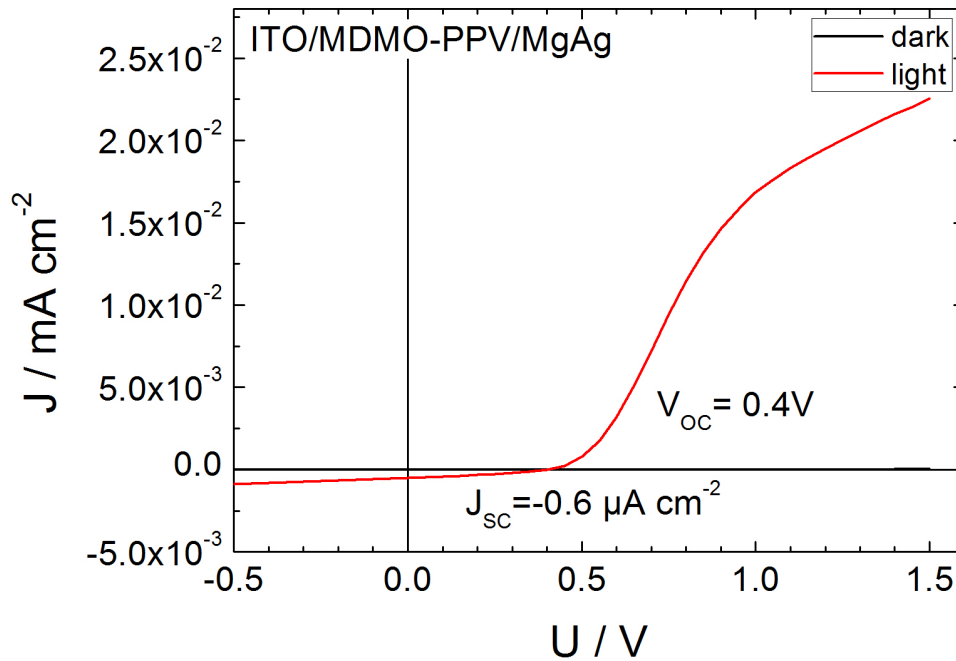
Figure 3.3.12:   Current density versus voltage, linear plot of an intrinsic MDMO-PPV/MgAg device
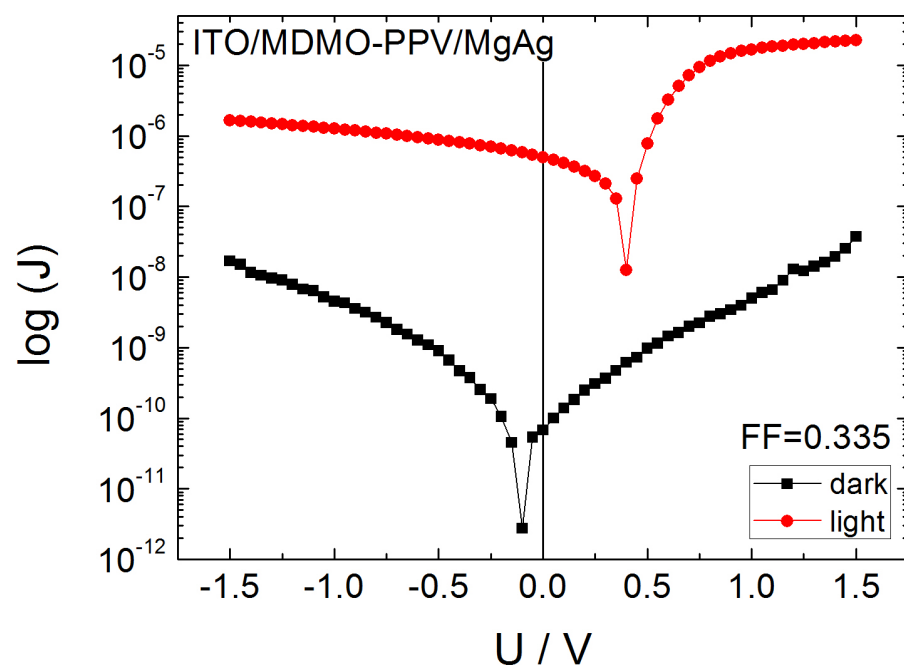
Figure 3.3.13:   Logarithmic plot of an intrinsic MDMO-PPV/MgAg device
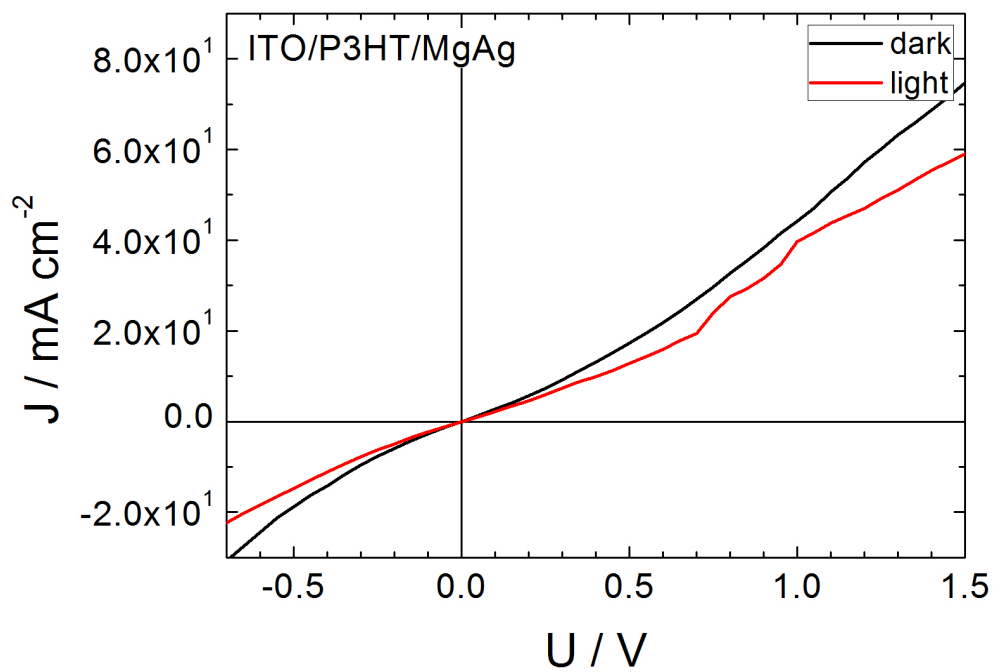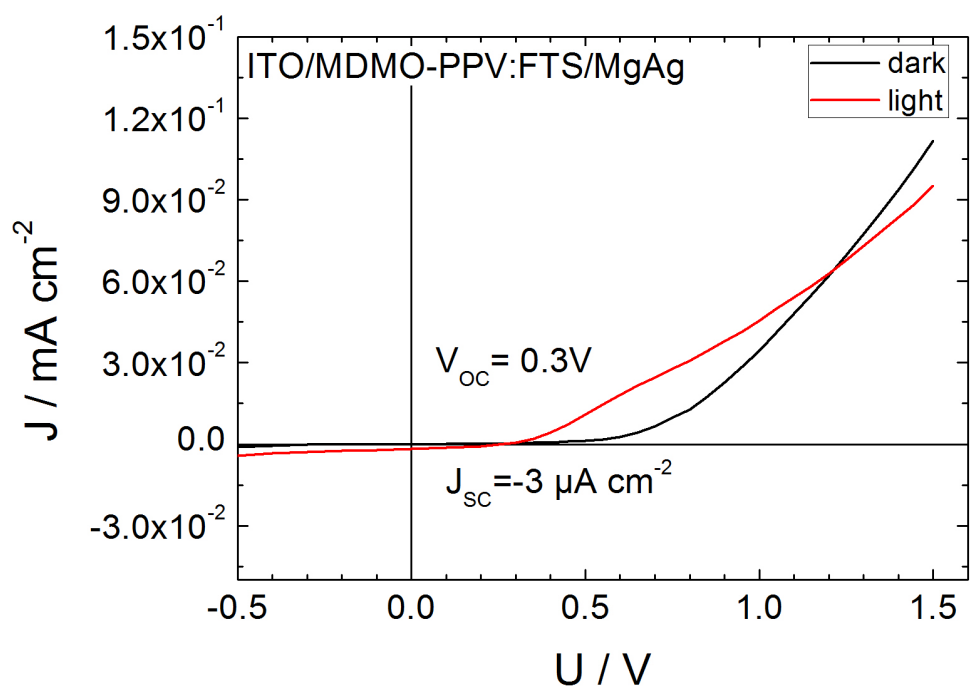
Figure 3.3.14:   Current density versus voltage, linear plot of a doped MDMO-PPV/MgAg
           device
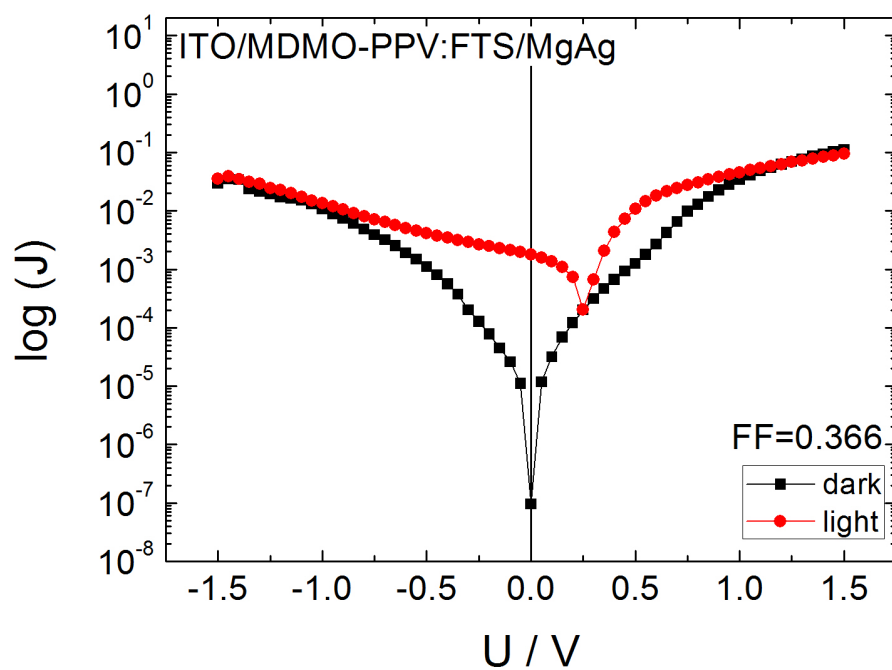
Figure 3.3.15:   Logarithmic plot of a doped MDMO-PPV/MgAg device

Devices with electrodes of magnesium/silver show a sufficient diode behavior (figures 3.3.12, 3.3.13, 3.3.14 and 3.3.15).

Nevertheless devices with samarium electrodes reach much higher open circuit potentials than magnesium/silver or aluminum samples (figures 3.3.16, 3.3.21, 3.3.18 and 3.3.23). Intrinsic devices behave like it was observed for P3HT/Al and MDMO-PPV/MgAg. Illumination enhances rectification.

Figure 3.3.16:   Current density versus voltage, linear plot of an intrinsic MDMO-PPV/Sm device

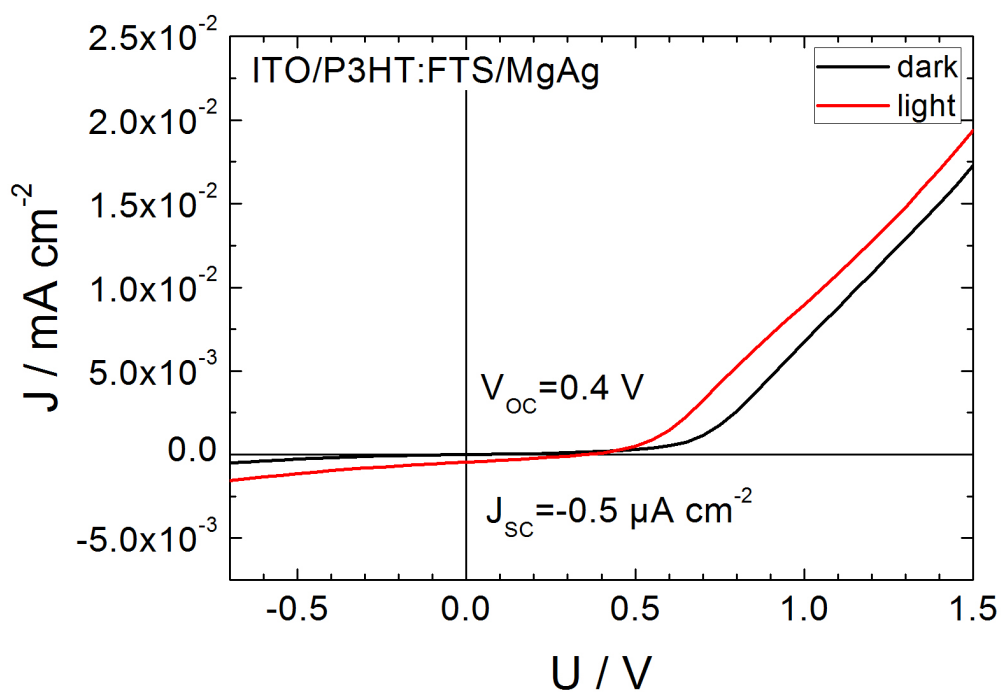Figure 3.3.17: Logarithmic plot of an intrinsic MDMO-PPV/Sm device

Figure 3.3.18:   Current density versus voltage, linear plot of a doped MDMO-PPV/Sm
device

Figure 3.3.19:   Logarithmic plot of a doped MDMO-PPV/Sm device

Although aluminum devices are more stable, compared to samarium and magnesium/silver devices, which are either oxidized easily or exhibit a low reproducibility, rectification is worse than for other electrodes but still sufficient.
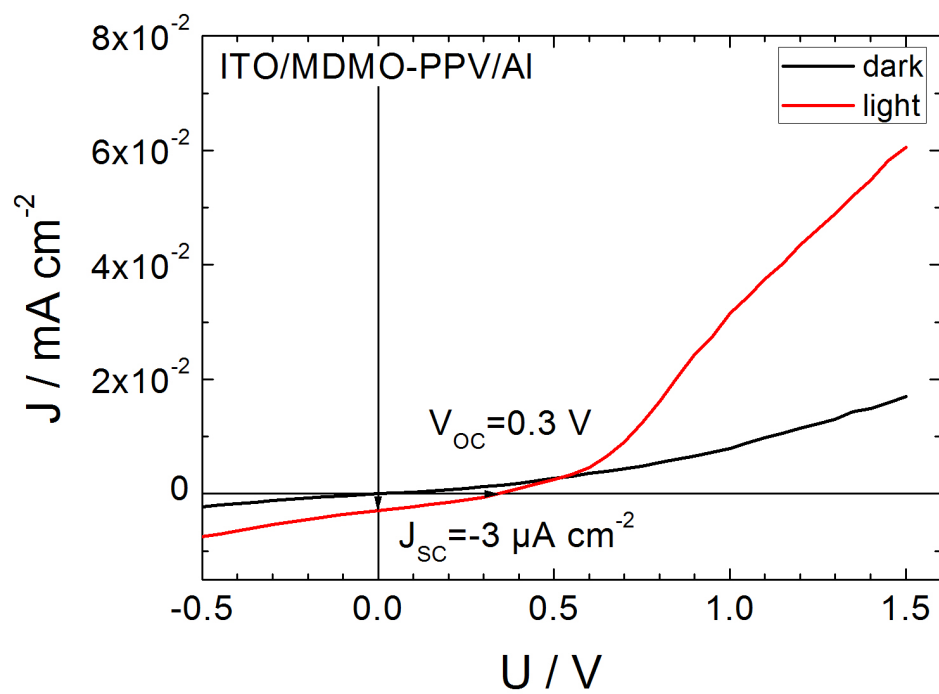
Figure 3.3.20:   Current density versus voltage, linear plot of an intrinsic MDMO-PPV/Al device
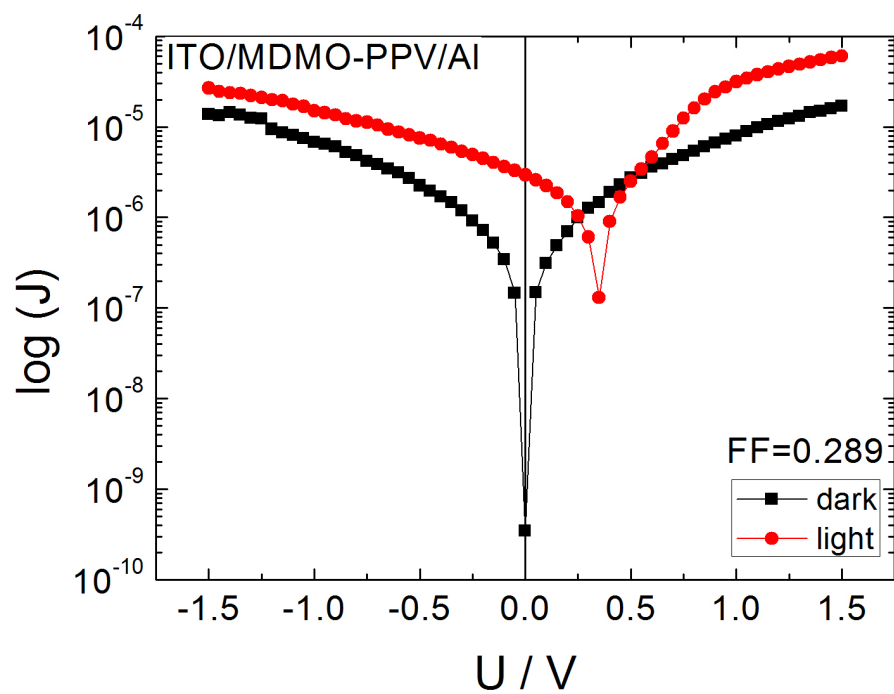
Figure 3.3.21:   Logarithmic plot of an intrinsic MDMO-PPV/Al device

Figure 3.3.22:   Current density versus voltage, linear plot of a doped MDMO-PPV/Al device
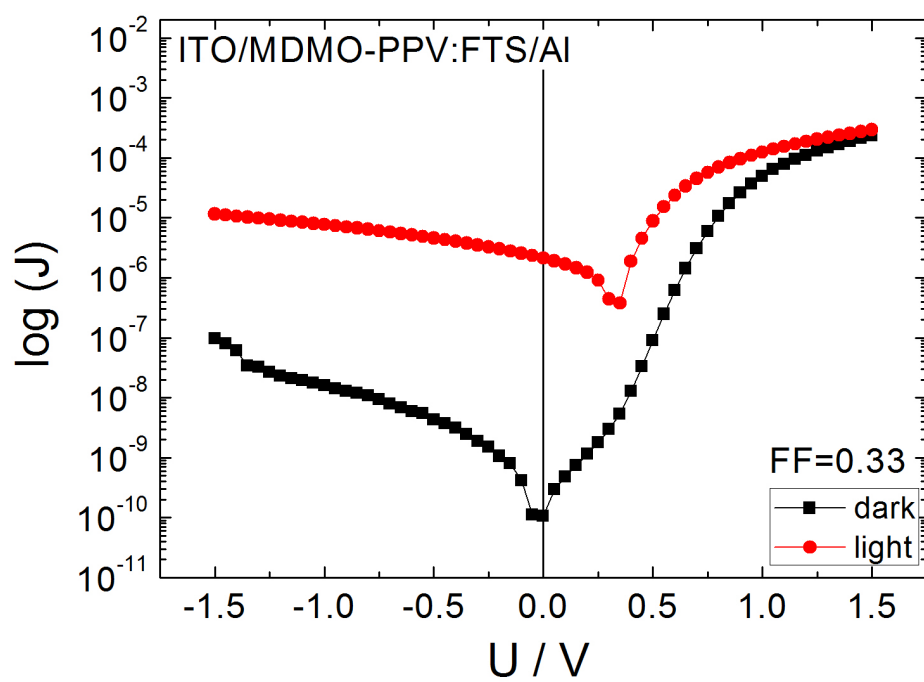
Figure 3.3.23:   Logarithmic plot of a doped MDMO-PPV/Al device

3.3.2.2 Mott Schottky Analysis

In Addition to favorable IV Characteristics, MDMO-PPV shows promising results in Mott
Schottky analysis. Therefore the work functions of these metals have to be positioned in
a good relationship with the HOMO and LUMO of the semiconductor. For aluminum and
samarium electrodes this restriction is given well. Also Mg/Ag would fulfill, nevertheless
impedance measurement did not show any sufficient results. The behavior of Mg/Ag devices
should be studied in further investigations.

Similar to P3HT, intrinsic MDMO-PPV does not contain enough respectively constant
charge carriers concentration and therefore does not show a sufficient linear regime of the
slope (Figure 3.3.27 and 3.3.24). As a consequence N_A was not determined for undoped Al
devices and undoped Sm devices.
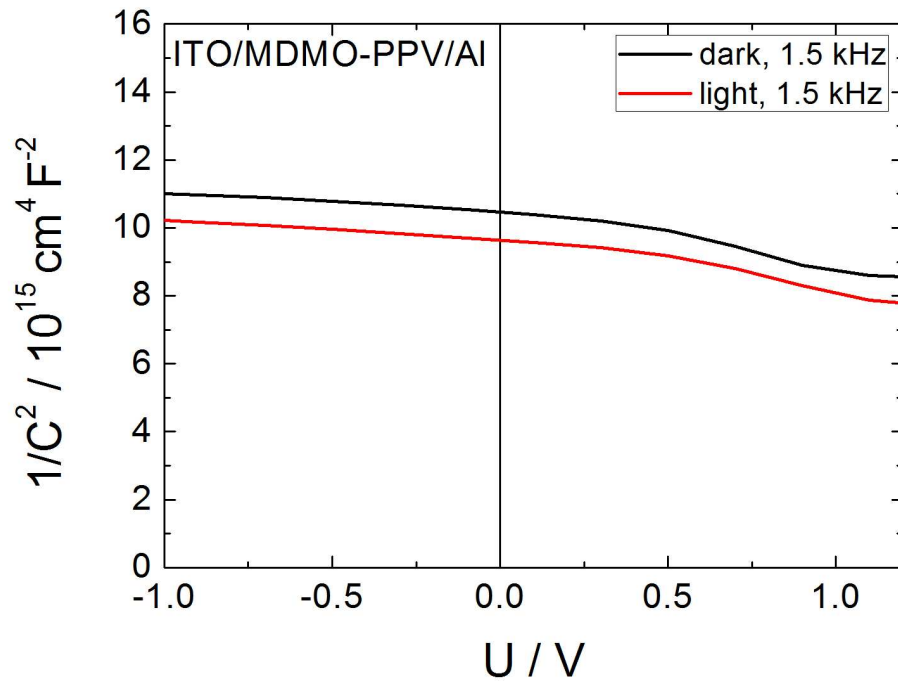
Figure 3.3.24: $1/C^2$ versus voltage plot of an intrinsic MDMO-PPV/Al device
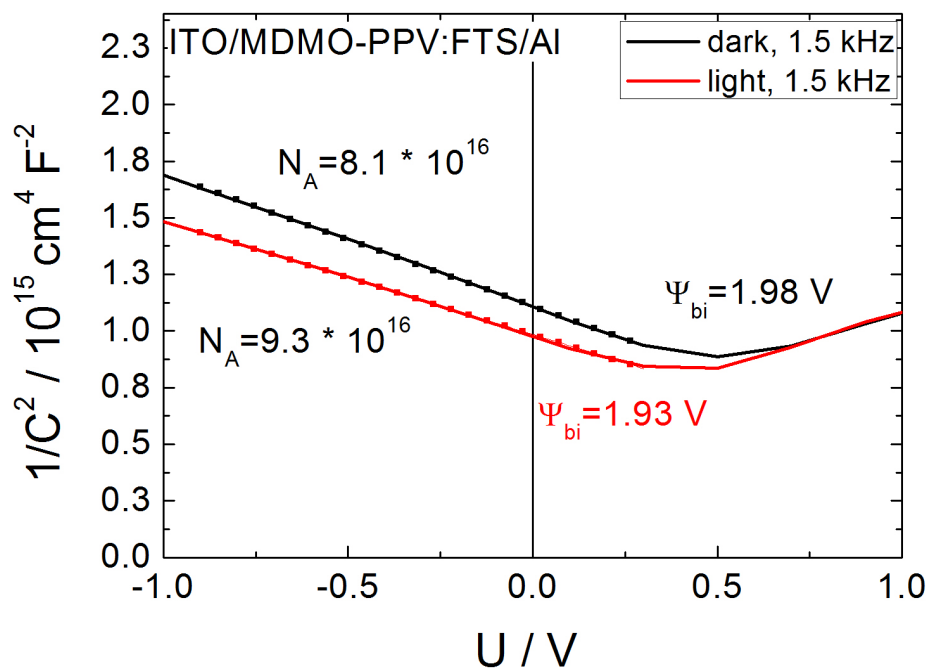
Figure 3.3.25: $1/C^2$ versus voltage plot of a doped MDMO-PPV/Al device

For MDMO-PPV:FTS/Al diodes a linear decrease of $1/C^2$ is observed. Therefore the charge carrier concentration was determined. Nevertheless the slope does not intersect with the x-axis at y=0, which might be due to inhomogenous charge carrier concentration. In contrast to P3HT, MDMO-PPV layers exhibited layer thicknesses of about 450 nm. For this thickness an exposure time to the dopant of 10 min could have been to short. The built-in potential was determined from the extrapolation of the slopes since values were still reasonable. For aluminum devices ψ_{bi} of 1.98 V in dark and 1.93 V under light excitation are observed. The depletion width of a doped Al device for the dark measurement is 90 nm and for the measurement with light excitation 83 nm.

Figure 3.3.26:   Plots of $1/C^2$ vs. voltage of intrinsic and doped MDMO-PPV capped with Al are compared. The plot of the doped device shows a typical Mott Schottky behavior with linear regime in contrast to the intrinsic device.
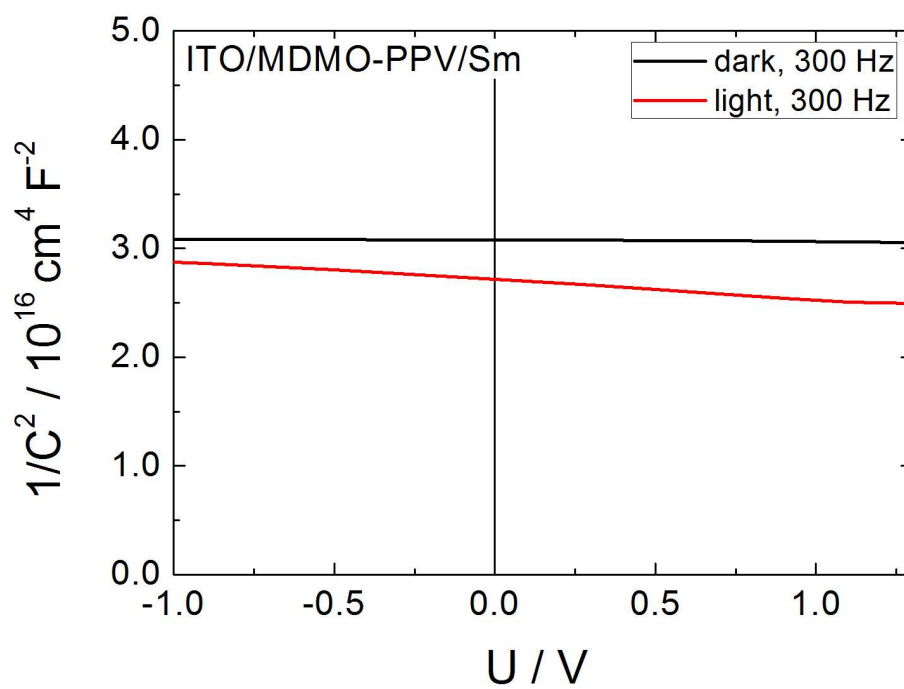
Figure 3.3.27: $1/C^2$ versus voltage plot of an intrinsic MDMO-PPV/Sm device
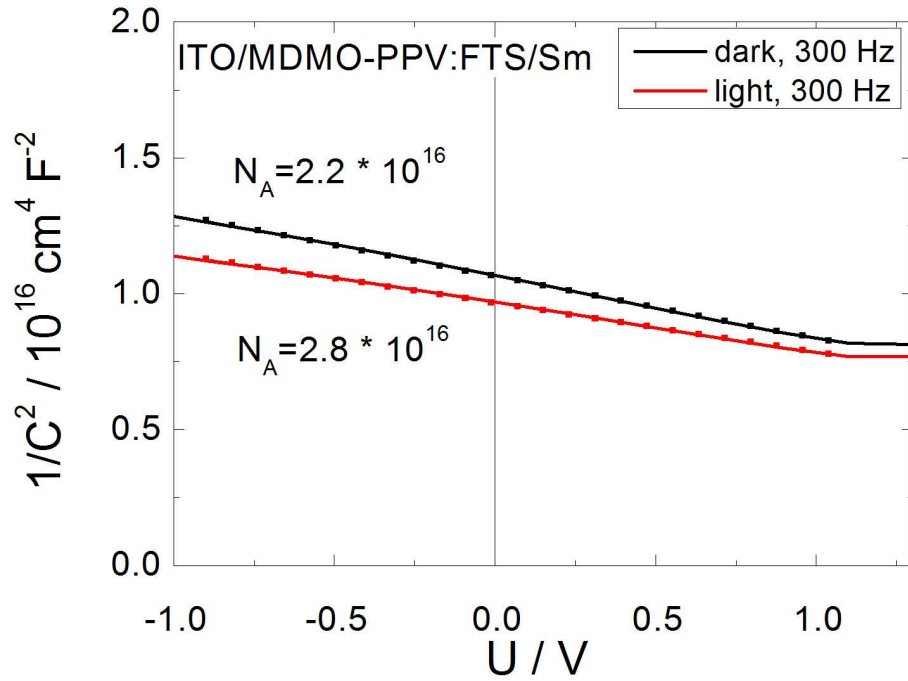
Figure 3.3.28: $1/C^2$ versus voltage plot of a doped MDMO-PPV/Sm device

For both metals a Schottky behavior is observed for the doped devices. Charge carrier concentrations were determined in the range of 10^{16} cm^{-3}. Built-in potentials of samarium devices could not be determined due to low capacities and as a result rather high $1/C^2$ values. It is expected that inhomogenous charge carrier distribution is the reason for missing intersection of the slope with the x-axis, as already mentioned for doped MDMO-PPV/Al devices.
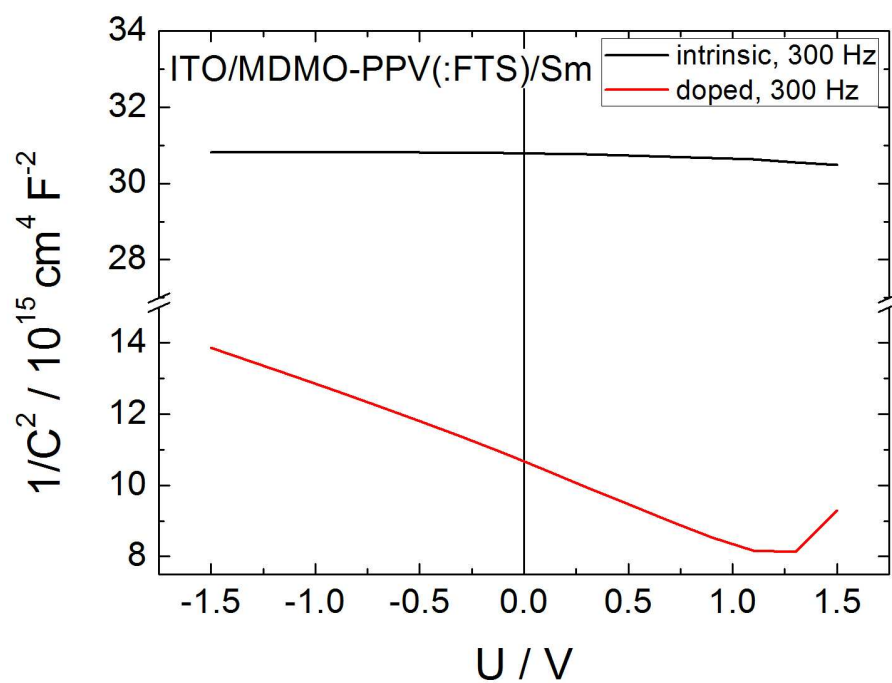
Figure 3.3.29:   Plots of $1/C^2$ vs. voltage of intrinsic and doped MDMO-PPV capped with Sm are compared. The plot of the doped device shows a typical Mott Schottky behavior with linear regime.

3.3.3 Zinc phtalocyanine devices

3.3.3.1 Current-Voltage Characteristics

In contrast to devices of the polymers P3HT and MDMO-PPV, ZnPc is very sensitive to metal evaporation. The metal complex structure behaves like a sponge and in addition evaporation of the semiconductor is limited by the amount of source material and due to this limited in film thickness (40 nm). As a result many devices showed short circuits, especially those having samarium and magnesium/silver electrodes. Therefore only devices with aluminum electrodes are discussed.

With illumination doped as well as intrinsic ZnPc devices behave slightly like a counter diode. A small rectification is observed against the ITO bottom electrode.
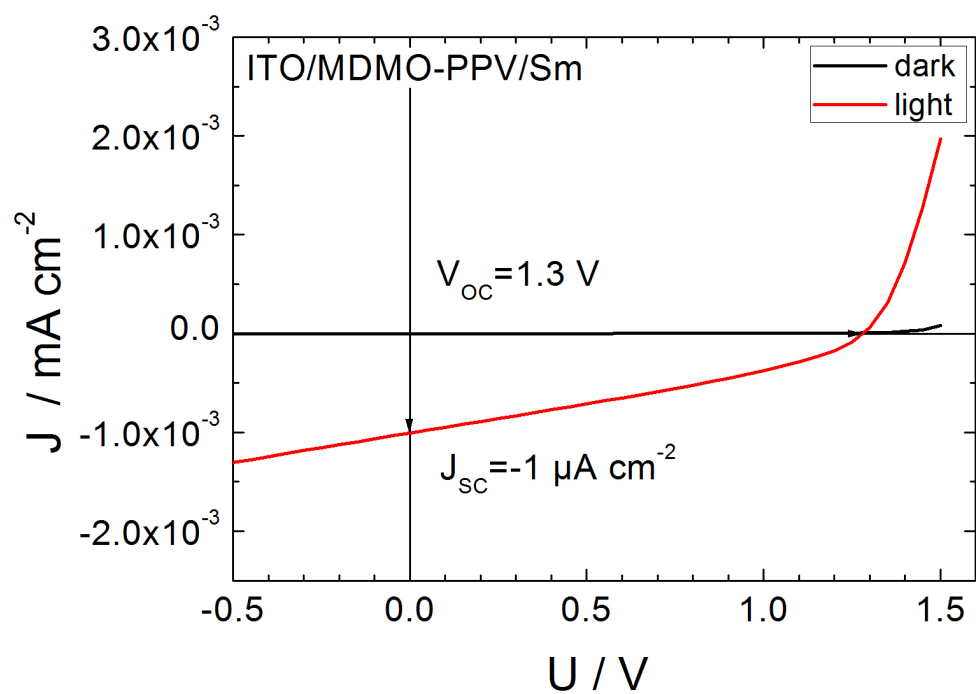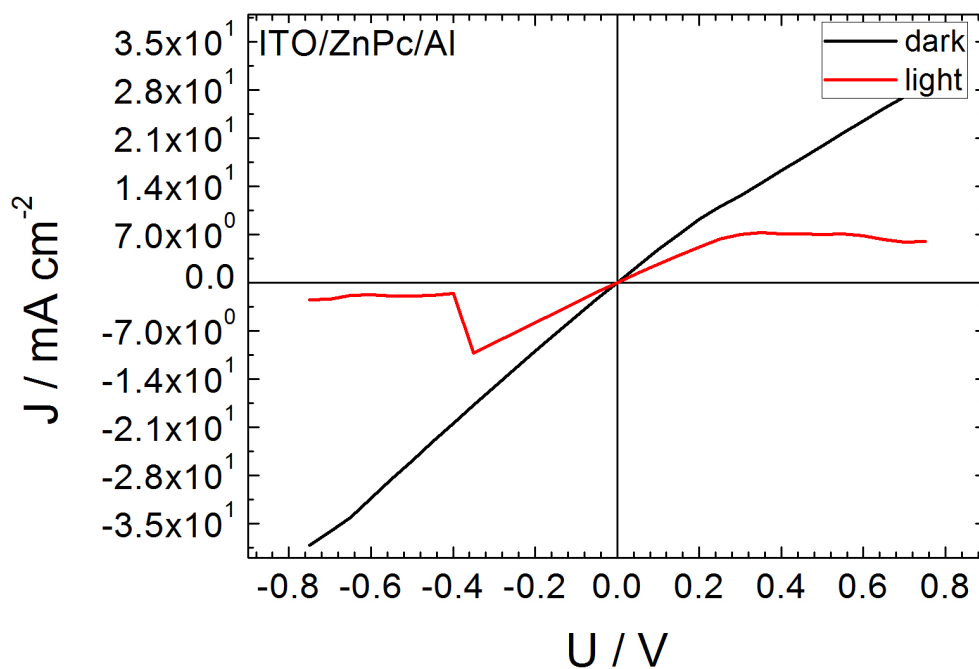

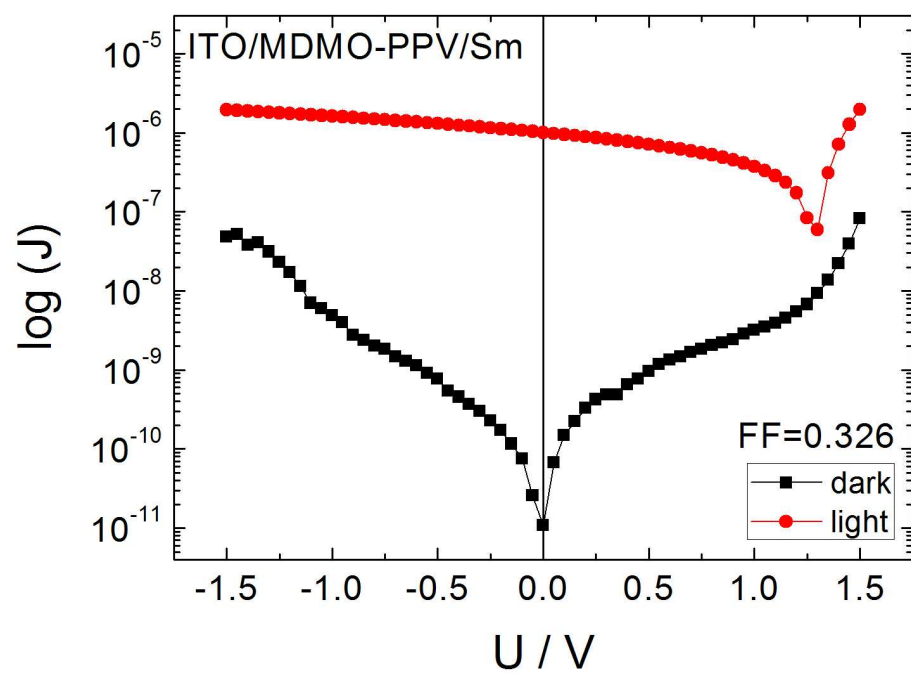Figure 3.3.30:   Current density versus voltage, linear plot of an intrinsic ZnPc/Al device
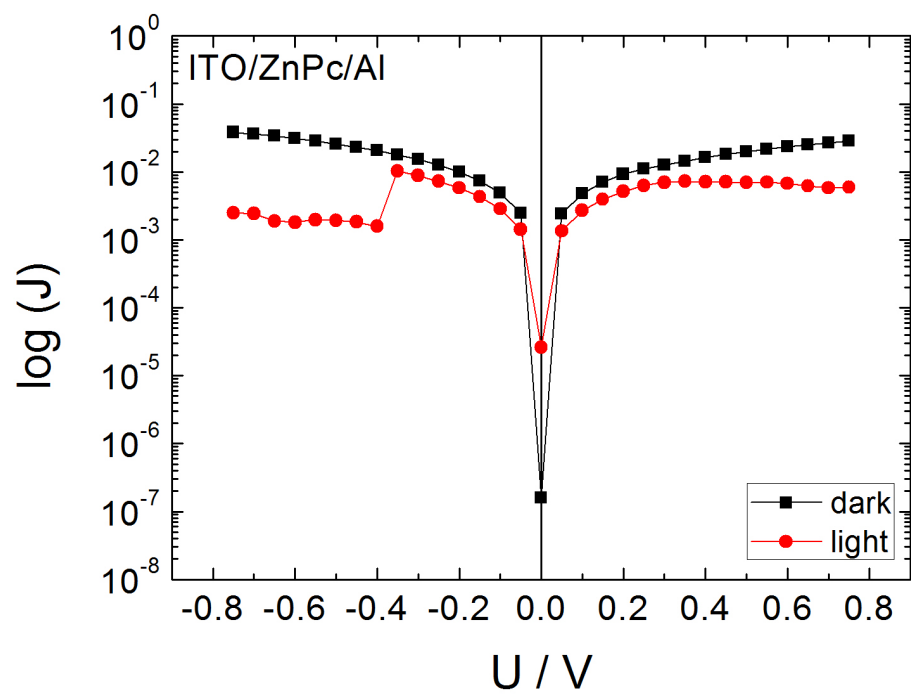
Figure 3.3.31:   Logarithmic plot of an intrinsic ZnPc/Al device
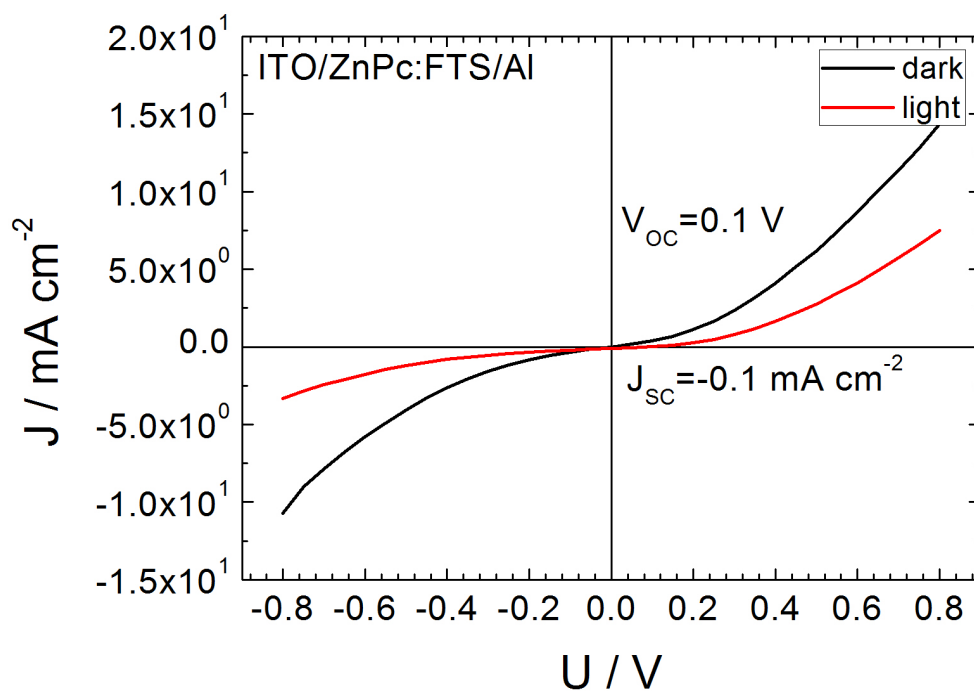
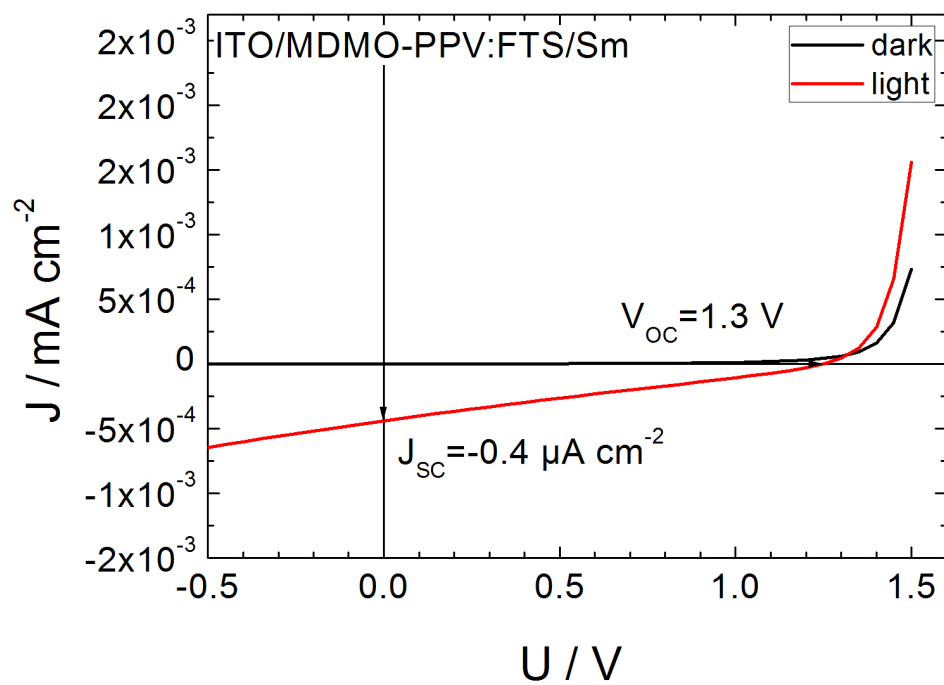Figure 3.3.32:   Current density versus voltage, linear plot of a doped ZnPc/Al device
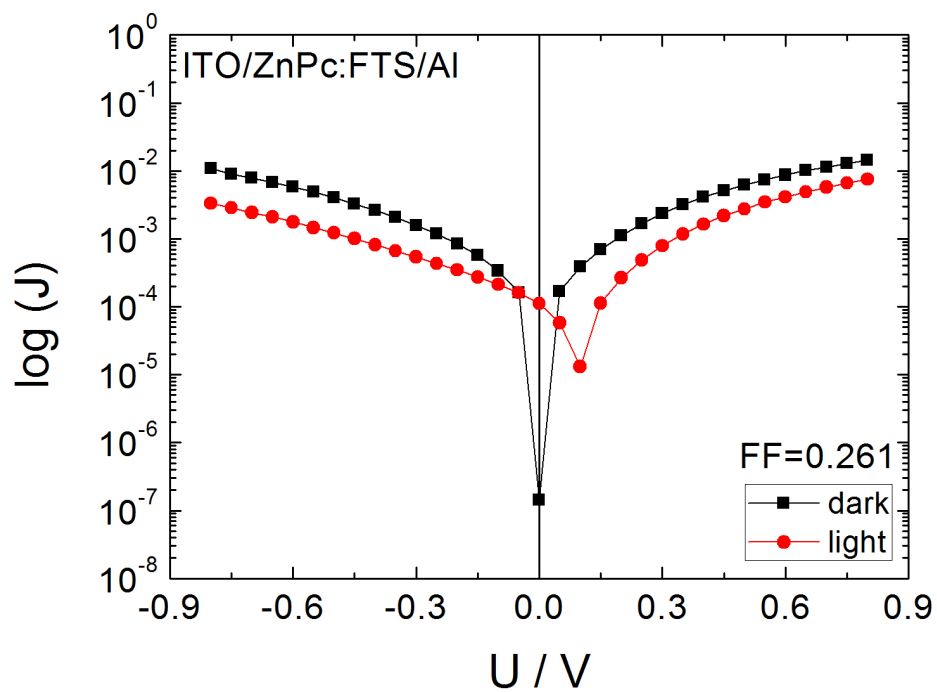
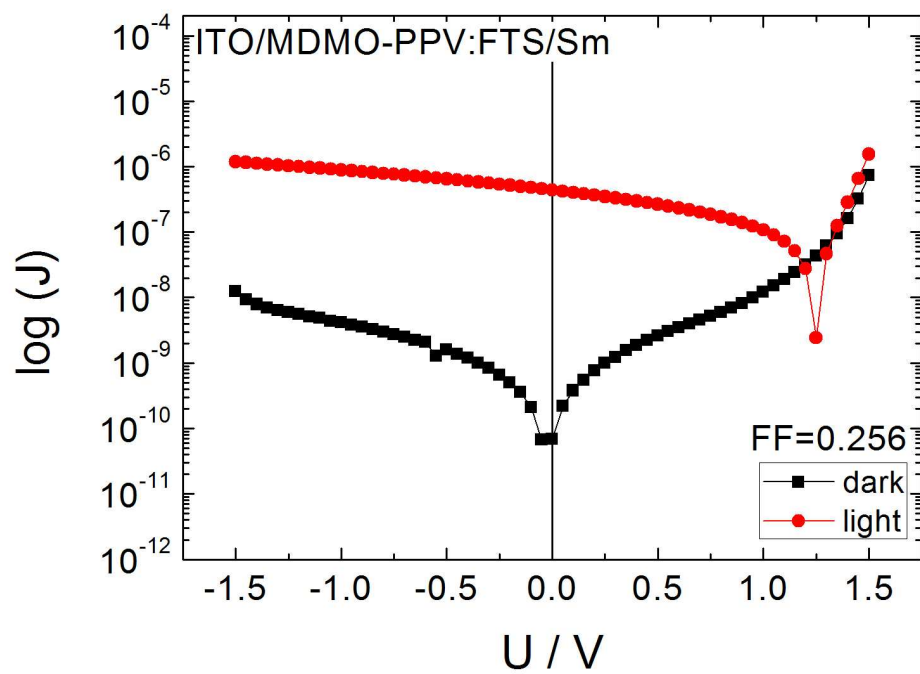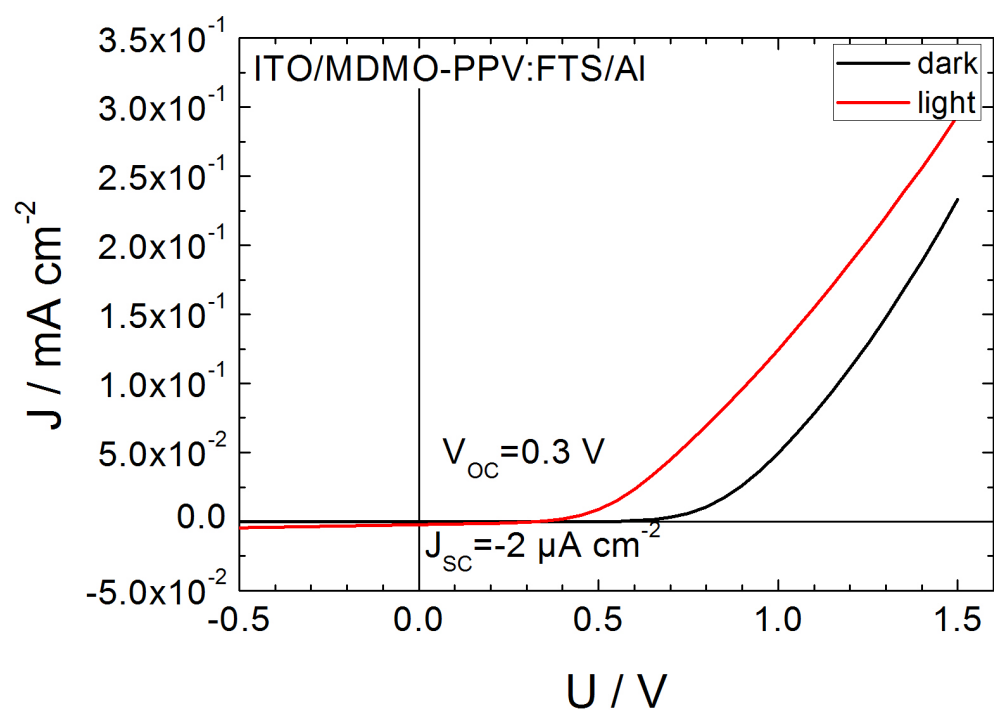Figure 3.3.33:   Logarithmic plot of a doped ZnPc/Al device

As seen for aluminum devices of P3HT (Figures 3.3.1, 3.3.2 and 3.3.3, 3.3.4) only doped ZnPc devices show a photovoltaic effect. In addition doping of the semiconductor indicates enhanced diode like behavior.

3.3.3.2 Mott Schottky analysis

Mott Schottky analysis of ZnPc devices feature a rather small linear regime. Impedance measurements as well as IV-measurements showed short circuits at voltages above 0.8 V and where therefore performed below. Again there is not observed any constant charge carrier concentration for the intrinsic device.
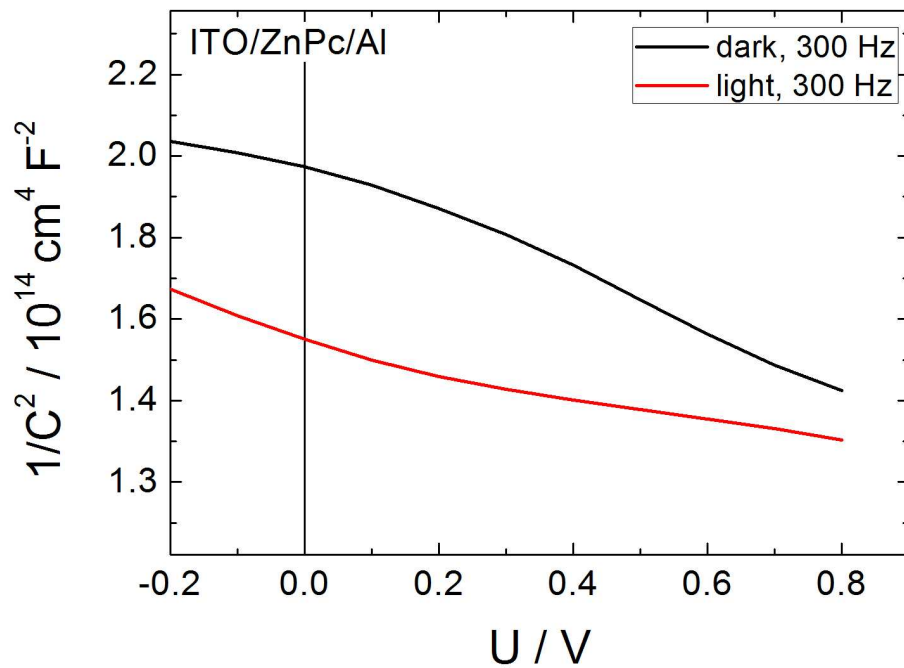
Figure 3.3.34: $1/C^2$ versus voltage plot of an intrinsic ZnPc/Al device
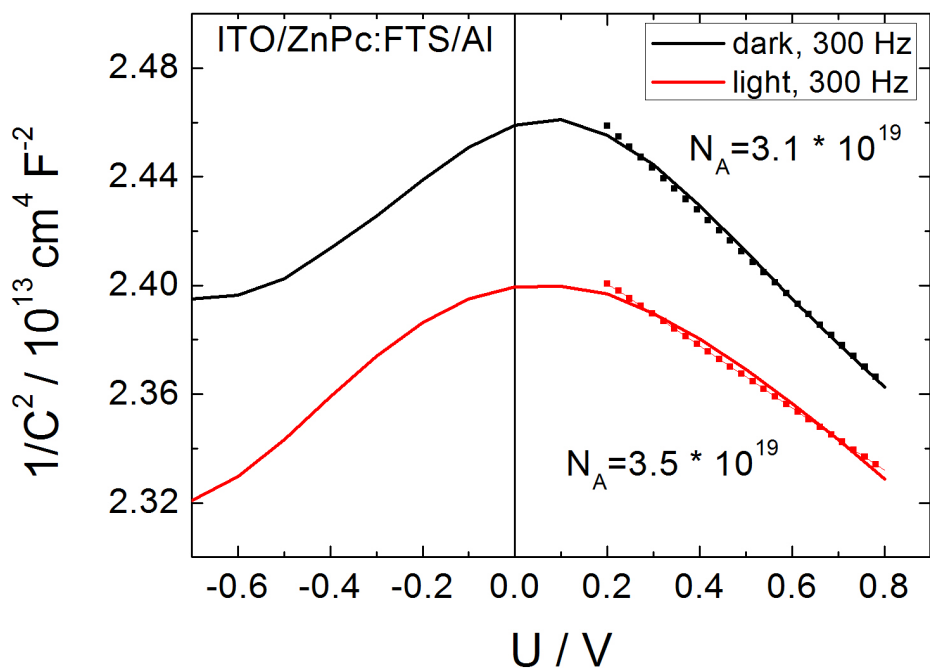
Figure 3.3.35: $1/C^2$ versus voltage plot of a doped ZnPc/Al device

As already discussed for IV-characteristics, ZnPc devices are expected to act as a counter diode against ITO. If one regards the Mott-Schottky analysis and the turned around graph one could expect that ZnPc forms a Schottky contact with ITO.

If this effect is regarded as not reasonable but the linear regime is interpreted as sufficient enough for Mott Schottky analysis, despite a very small capacitance regime, ZnPc devices would show the highest charge carrier concentration per volume, in comparison to P3HT and MDMO-PPV. High charge carrier concentration is the proof for a rather strong doping compared to samples with polymers. In addition this investigation would be supported by the fact of color change after doping (figure 3.2.5) which is not observed for P3HT and MDMO-PPV devices. It appears that the linear regime is in a very small capacitance regime and can be regarded as constant. Therefore indication as Schottky contact is not suggestive. The counter diode behavior should be investigated more detailed since also IV-characteristics point at such an effect.

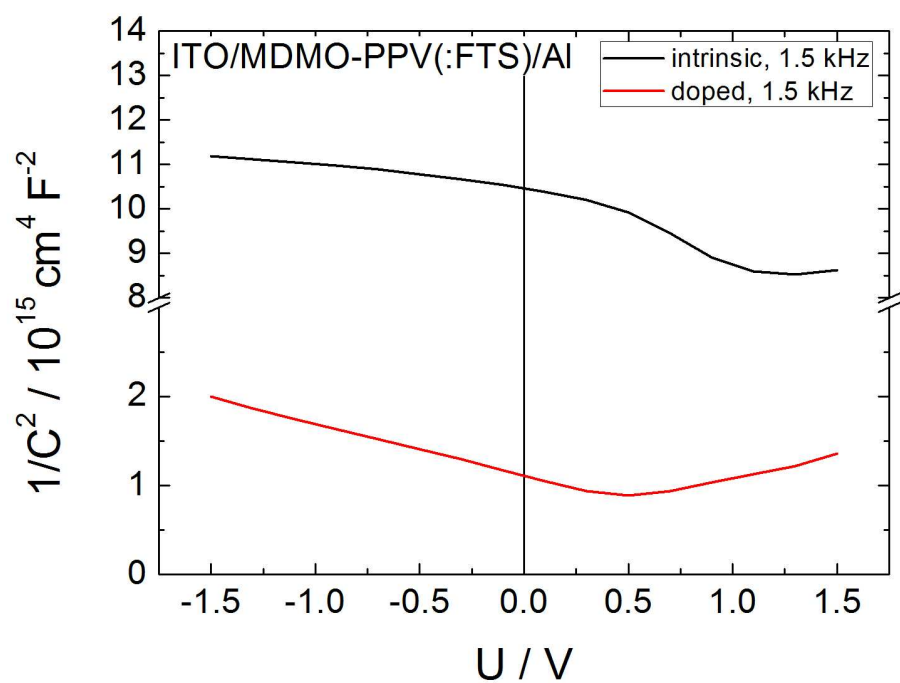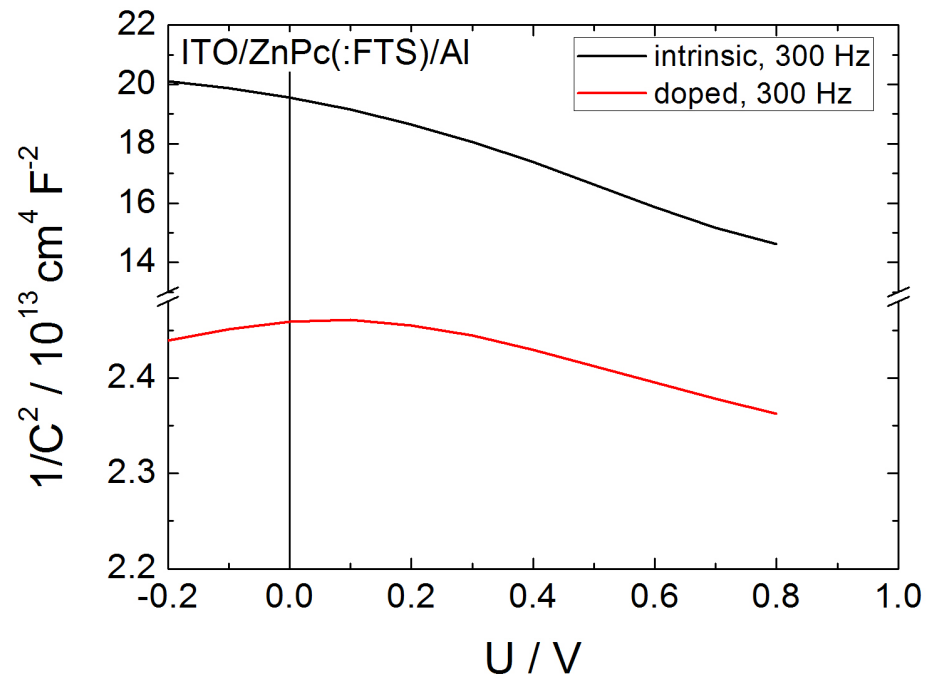Figure 3.3.36: Comparison of $1/C^2$ vs. voltage plots of intrinsic and doped ZnPc capped with Al. The plot of the doped device shows a typical Mott Schottky behavior with linear regime.

4 Conclusion and Discussion

From the results of this study a small overview for Schottky junctions between the organic semiconductors P3HT, MDMO-PPV and ZnPc and several metals is gained.

From the investigations in IV-measurements it is seen that the doping of semiconductors does not achieve any big changes in photovoltaic effects of the diodes. This is observed by regarding table 4.1, which compares open circuit potentials of intrinsic devices and doped ones.

material	metal	intrinsic	doped
P3HT	Al	0.2	0.1
	Mg/Ag	0	0.4
MDMO-PPV	Al	0.3	0.3
	Sm	1.3	1.3
	MgAg	0.4	0.3
ZnPc	Al	0	0.1

Table 4.1: Comparison of open circuit potentials V_{OC} of different devices

Open circuit potentials of doped MDMO- PPV and ZnPc devices are negligibly lower than the V_{OC} of intrinsic devices. P3HT devices do not show a distinct tendency. Nevertheless it is revealed that the diode behavior (higher forward bias) of all devices is enhanced through doping, comparing IV curves of intrinsic and doped diodes.

Changes of typical absorption features and further quenching was observed in UV-Vis and photoluminescence measurements after doping. These results initiated further investigation with FTIR measurements. From FTIR results it is seen as evidence that our chosen pathway of chemical induced charge carriers with a fluorinated alkylsilane is classed as a doping process. FTIR features of FTS doping show polaronic absorption and IRAV features as well, but from time dependent measurements it is obvious that FTS doping is a rather slow and slightly doping process compared to iodine doping (figure 4.0.1). After detailed investigations during this study it is expected that FTS is reduced during doping. Fluorine and chlorine atoms from the alkyl chain might act as electron acceptors due to their high electronegativity. Nevertheless the exact reaction pathway has to be studied more detailed and i has to be proofed.

(a)

(b)
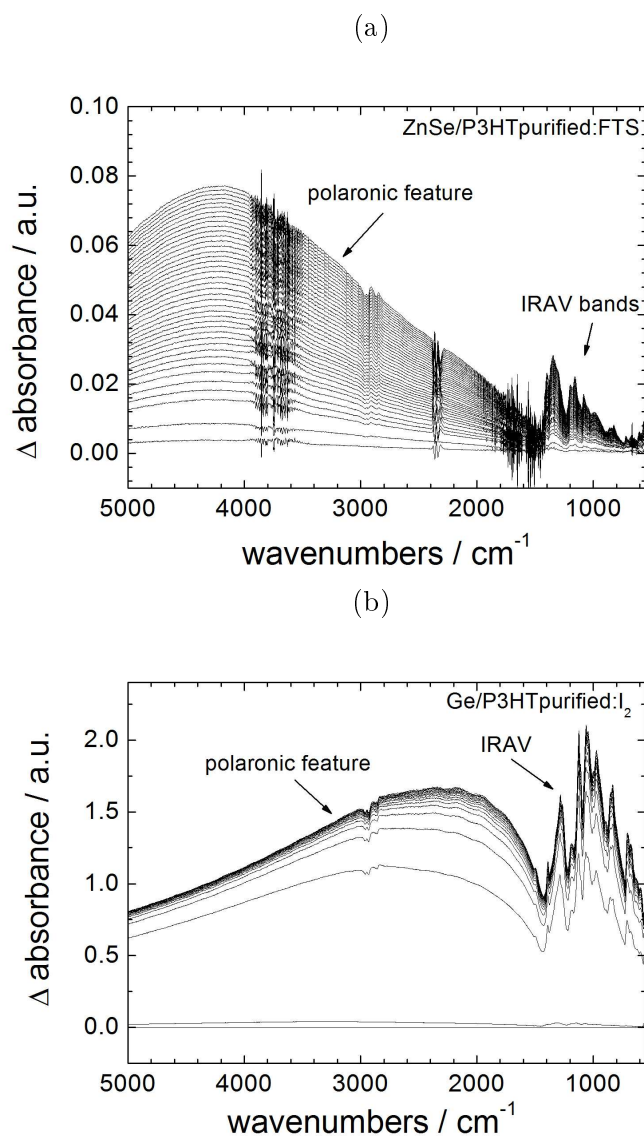
Figure 4.0.1:   FTIR spectra of FTS doping (a) and iodine doping (b) showing the same features: polaronic absorption between 1500 cm^{-1} and 5000 cm^{-1}, IRAV bands below 1500 cm^{-1}

The insight of slow and slight doping is an important fact for generation of Schottky junctions.

Table 4.2 displays all results from Mott-Schottky analysis. The most stable devices, first and foremost aluminum devices, show promising results.

device	mode	d [nm]	$N_A[cm^{-3}]$	ω [nm]	$\psi_{bi}[V]$
P3HT:FTS/Al	dark	80	$3.3 \cdot 10^{17}$	31	0.71
	light	80	$3.3 \cdot 10^{17}$	29	0.54
MDMO-PPV:FTS/Al	dark	450	$8.01 \cdot 10^{16}$	90	1.98
	light	450	$9.3 \cdot 10^{16}$	83	1.93
MDMO-PPV:FTS/Sm	dark	450	$2.2 \cdot 10^{16}$	/	/
	light	450	$2.8 \cdot 10^{16}$	/	/
ZnPc:FTS/Al	dark	40	$3.1 \cdot 10^{19}$	/	/
	light	40	$3.5 \cdot 10^{19}$	/	/

Table 4.2:   Comparison of results from impedance measurements

Comparison of results from table 4.2 indicates a connection between thin film thickness of the semiconductor and charge carrier concentration. The carrier concentration increases with thin film thickness. Though the exposition time of devices to the doping vapor was varied depending on film thickness, the thinnest films (ZnPc and P3HT) appear to feature the highest carrier concentration per volume. It is expected that fluorinated alkylsilanes incorporate into organic semiconductor thin films, which is more sufficient for lower thickness of thin films.

Beneath charge carrier concentration, depletion width and built in potential of the devices were determined using Mott-Schottky analysis. These quantities could only be defined for results with low enough capacities respectively homogenous charge carrier distribution, low voltage ranges (at higher voltages short circuits were observed) and certain frequencies. MDMO-PPV/Sm and ZnPc/Al devices show high $1/C^2$ values and the intersection of the slope with the x-axis at y=0 is missing, therefore the built in potential could not be determined. For the other devices reasonable values for depletion width and built in potential were achieved.

This study shows the efficiency of Schottky diodes using P3HT, MDMO-PPV and ZnPc. MDMO-PPV gives promising devices, indifferent which metal was chosen for the junction. MDMO-PPV is favorable due to easy handling (spin coating of solution), air stability (does not degrade in air like P3HT) and surface morphology of thin films (smooth thin films) (figure 3.1.2).

Besides MDMO-PPV also ZnPc devices show promising results, regarding results from IV-measurements (figures 3.3.30 and 3.3.32). Impedance measurements are supposed to be reinvestigated closer and optimized. Parameters like thin film thickness of ZnPc, exposition time to the doping vapor or variation of the capping metal respectively alloys should be investigated more precisely.

As a very important insight, doping with FTS has to be regarded. It is necessary to gain deeper knowledge in how the doping mechanism works exactly and how exact control can be achieved, for example by advancing the petri-dish method to a sophisticated doping setup. This doping method is expected to offer a wide range of applications and constitutes a possibility for controllable chemical doping.

5 Symbols and Abbreviations

$q\psi_{bi}$, ψ	.....	built-in energy [J], built-in potential [V]
V, $V_{applied}$	.....	applied potential [V]
$q\Phi_M$	.....	workfunction of the metal [eV]
χ	.....	electron affinity
ω	.....	depletion width [nm]
d	.....	thickness of semiconductor layer [nm]
E_F	.....	Fermi level [J]
E	.....	electric field
E_C	.....	Coulomb potential
k	.....	Boltzmann constant ($1.38 \cdot 10^{-23}$ J/K)
T	.....	temperature (K)
ε	.....	permittivity (C $V^{-1}m^{-1}$)
ε_0	.....	permittivity of vacuum ($8.85 \cdot 10^{-12}$ C $V^{-1}m^{-1}$)
ε_S	.....	dielectric constant (relative permittivity)
		of the semiconductor (dimensionless) (table 2.2)
q	.....	elementary charge ($1.602 \cdot 10^{-19}$ C)
q_1, q_2	.....	charge
r	.....	radius, distance
N_A	.....	concentration of charge carriers, A referring to acceptors [cm^{-3}]
k	.....	slope
HOMO	.....	highest occupied molecular orbital of the polymer
		(corresponds to the valence band of a semiconductor E_V)
LUMO	.....	lowest unoccupied molecular orbital of the polymer
		(corresponds to the conduction band of a semiconductor E_C)
C, C_A	.....	capacity [F], capacity per area [F cm^{-2}]
P3HT	.....	poly-(3-hexylthiophene)
MDMO-PPV	.....	poly-[2-methoxy-5-(3', 7'-dimethyloctyl)-p-phenylene-vinylene]
ZnPc	.....	zinc phtalocyanine
MEH-PPV	.....	poly-[2-methoxy-5-(2'-ethylhexyloxy)-p-phenylene vinylene]
F4-TCNQ	.....	2,3,5,6-tetrafluoro-7,7',8,8'-tetracyanoquinodimethane
ITO	.....	indium-tin-oxide

5 Symbols and Abbreviations

FTS	.....	tridecafluoro-(1,1,2,2-tetrahydrooctyl)-trichlorosilane
AFM	.....	atomic force microscope
FTIR	.....	Fourier transform infrared
IV	.....	current-voltage
IRAV	.....	infrared activated vibration
UV-Vis	.....	ultraviolet-visible
V_{OC}	.....	open circuit potential [V]
J_{SC}	.....	short circuit current density [A cm^{-2}]

Bibliography

[1] J. Bisquert, G. Garcia-Belmonte, A. Munar, M. Sessolo, A. Soriano, and H. J. Bolink. Band unpinning and photovoltaic model for P3HT:PCBM organic bulk heterojunctions under illumination. *Chemical Physics Letters*, 465(1-3):57–62, November 2008.

[2] C. J. Brabec, N. S. Sariciftci, and J. C. Hummelen. Plastic Solar Cells. *Advanced Functional Materials*, 11(1):15–26, February 2001.

[3] J. L. Brédas and R. Silbey. *Conjugated Polymers*. Kluwer Academic Publishers, 1991.

[4] Gilles Dennler, Christoph Lungenschmied, Niyazi Serdar Sariciftci, Reinhard Schwoediauer, Siegfried Bauer, and Howard Reiss. Unusual electromechanical effects in organic semiconductor Schottky contacts: Between piezoelectricity and electrostriction. *Applied Physics Letters*, 87(16):163501, 2005.

[5] Gilles Dennler, Niyazi Serdar Sariciftci, Reinhard Schwoediauer, Siegfried Bauer, and Howard Reiss. Unexpected electromechanical actuation in conjugated polymer based diodes. *Journal of Materials Chemistry*, 16(19):1789–1793, 2006.

[6] Yong Seok Eo, Hee Woo Rhee, Byung Doo Chin, and Jae-Woong Yu. Influence of metal cathode for organic photovoltaic device performance. *Synthetic Metals*, 159(17-18):1910–1913, September 2009.

[7] G Garciabelmonte, a Munar, E Barea, J Bisquert, I Ugarte, and R Pacios. Charge carrier mobility and lifetime of organic bulk heterojunctions analyzed by impedance spectroscopy. *Organic Electronics*, 9(5):847–851, October 2008.

[8] Ali Bilge Guvenc, Emre Yengel, Guoping Wang, Cengiz S. Ozkan, and Mihrimah Ozkan. Effect of incident light power on Schottky barriers and I-V characteristics of organic bulk heterojunction photodiodes. *Applied Physics Letters*, 96(14):143301, 2010.

[9] B H Hamadani, H Ding, Y Gao, and D Natelson. Doping dependent charge injection and band alignment in organic field-effect transistors. *Exposure*, pages 2–6.

[10] A. J. Heeger, N. S. Sariciftci, and E. B. Namdas. *Semiconducting and Metallic Polymer*. Oxford University Press, 1st editio edition, 2010.

[11] Chi Yueh Kao, Bumsu Lee, Leszek S. Wielunski, Martin Heeney, Iain McCulloch, Eric Garfunkel, Leonard C. Feldman, and Vitaly Podzorov. Doping of Conjugated Polythiophenes with Alkyl Silanes. *Advanced Functional Materials*, 19(12):1906–1911, June 2009.

[12] O. Khatib, B. Lee, J. Yuen, Z. Q. Li, M. Di Ventra, a. J. Heeger, V. Podzorov, and D. N. Basov. Infrared signatures of high carrier densities induced in semiconducting poly(3-hexylthiophene) by fluorinated organosilane molecules. *Journal of Applied Physics*, 107(12):123702, 2010.

[13] C.S. Kuo, F.G. Wakim, S.K. Sengupta, and S.K. Tripathy. Schottky diodes using poly(3-hexylthiophene). *Journal of Applied Physics*, 74(4):2957–2958, 1993.

[14] Liang Ma, Wi Hyoung Lee, Yeong Don Park, Jong Soo Kim, Hwa Sung Lee, and Kilwon Cho. High performance polythiophene thin-film transistors doped with very small amounts of an electron acceptor. *Applied Physics Letters*, 92(6):063310, 2008.

[15] F. Maddalena, E. J. Meijer, K. Asadi, D. M. de Leeuw, and P. W. M. Blom. Doping kinetics of organic semiconductors investigated by field-effect transistors. *Applied Physics Letters*, 97(4):043302, 2010.

[16] Date J. D. Moet, L. Jan Anton Koster, Bert de Boer, and Paul W. M. Blom. Hybrid Polymer Solar Cells from Highly Reactive Diethylzinc: MDMO-PPV versus P3HT. *Chemistry of Materials*, 19(24):5856–5861, November 2007.

[17] Jan Obrzut and Kirt a. Page. Electrical conductivity and relaxation in poly(3-hexylthiophene). *Physical Review B*, 80(19):1–7, November 2009.

[18] D. B. A. Rep, A. F. Morpurgo, and T. M. Klapwijk. Doping-dependent charge injection into regioregular poly(3-hexylthiophene). *Organic Electronics*, 4(4):201–207, December 2003.

[19] R. H. Friend R.N. Marks, J.J.M. Halls, D.D.C. Bradley and A.B. Holmes. The photovoltaic response in poly(p-phenylene vinylene) thin-film devices. *Journal of Physics: Condensed Matter*, 6:1379–1394, 1994.

[20] Ajay Kumar Singh. *Electronic Devices and Integrated Circuits*. Prentice- Hall of India Private Limited, 2008.

[21] Vipul Singh, Anil Kumar Thakur, Shyam Sudhir Pandey, Wataru Takashima, and Keiichi Kaneto. Evidence of photoluminescence quenching in poly(3-hexylthiophene-2,5-diyl) due to injected charge carriers. *Synthetic Metals*, 158(7):283–286, May 2008.

[22] Sam-Shajing Sun and Niyazi Serdar Sariciftci. *Organic Photovoltaics: Mechanisms, Materials, and Devices*. CRC Press, 2005.

[23] S. M. Sze and Kwok K. Ng. *Physics of Semiconductor Devices*. Wiley, 3rd editio edition, 2007.

[24] S.M. Sze. *Semiconductor Devices: Physics and Technology*. Wiley, 1985.

Bibliography

[25] Ineke Van Severen, Martin Breselge, Sofie Fourier, Peter Adriaensens, Jean Manca, Laurence Lutsen, Thomas J. Cleij, and Dirk Vanderzande. 2,5-Substituted PPV-Derivatives with Different Polarities: The Effect of Side Chain Polarity on Solubility, Optical and Electronic Properties. *Macromolecular Chemistry and Physics*, 208(2):196–206, January 2007.

[26] W. Wojdyla, M., Derkowska, B., Lukasiak, Z., Bala. Absorption and photoreflectance spectroscopy of zinc phtalocyanine (ZnPc) thin films grown by thermal evaporation. *Material Letters*, 60:3441–3446, 2006.

[27] Minlu Zhang, Huanjun Ding, Yongli Gao, and C. W. Tang. Organic Schottky barrier photovoltaic cells based on MoO[sub x]/C[sub 60]. *Applied Physics Letters*, 96(18):183301, 2010.

[28] Yuan Zhang, Bert de Boer, and Paul W. M. Blom. Controllable Molecular Doping and Charge Transport in Solution-Processed Polymer Semiconducting Layers. *Advanced Functional Materials*, 19(12):1901–1905, June 2009.

Further reading

- S. Hamwi, J. Meyer, T. Winkler, T. Riedl, and W. Kowalsky. p-type doping efficiency of MoO_3 in organic hole transport materials. *Applied Physics Letters,* 94(25):253307, 2009.

- D. Comoretto, G. Dellepiane, F. Marabelli, J. Cornil, D. dos Santos, J. Brédas, D. Moses.Optical constants of highly stretch-oriented poly(p-phenylene-vinylene): A joint experimental and theoretical study. *Physical Review B*, 62(15):10173, 2000.

- M. Giulianini, E. R. Waclawik, J. M. Bell, N. Motta. Temperature and electric field dependent mobility in poly(3-hexylthiophene) diodes. *Journal of Applied Physics*, 108(1):014512, 2010.

- M. Green. Enhancement of Schottky solar cell efficiency above its semiempirical limit. *Applied Physics Letters*, 27(5):287, 1975.

- E. Itoh, K. Terashima, H. Nagai, K. Miyairi. Evaluation of poly(3-hexylthiophene)/polymeric insulator interface by charge modulation spectroscopy technique. *Thin Solid Films*, 518(2):810, 2009.

- P. Kumar, S. C. Jain, V. Kumar, S. Chand, R. P. Tandon. Effect of non-zero Schottky barrier on the J-V characteristics of organic diodes. *The European physical journal. E, Soft matter*, 28(4):361, 2009.

- S. Rajaputra, G. Sagi, V. P. Singh. Schottky diode solar cells on electrodeposited copper phthalocyanine films. *Solar Energy Materials and Solar Cells*, 93(1):60, 2009.

Bibliography

- Kim Kangdae, Koo Jaebon, Noh Yongyoung, Lee Jongkeun, Yang Yongsuk, and You Inkyu. Electric Characteristics of an Organic Schottky Diode according to Variation of P3HT Thickness. *Journal of the Korean Physical Society,* 57(1):124, 2010.

- Arash Takshi, Milad Mohammadi, and John D. Madden. Study the effect of distribution of density of states on the depletion width of organic Schottky contacts. *Solid-State Electronics,* 52(11):1717-1721, 2008.

- Toshihiro Yamanari, Tetsuya Taima, Jun Sakai, and Kazuhiro Saito. Highly Efficient Organic Thin-Film Solar Cells Based on poly(3-hexylthiophene) and Soluble C_{70} Fullerene Derivative. *Japanese Journal of Applied Physics,* 47(2):1230-1233, 2008.

- I.D. Parker. Carrier tunneling and device characteristics in polymer light-emitting diodes. *Journal of Applied Physics*, 75:1656-1666, 1994.

CURRICULUM VITAE

Stefanie Schlager
  Bruck 1
  4842 Zell am Pettenfirst, Austria
  Phone: 0664/5317538
  E-mail: stefanie.schlager@jku.at

Personal Data

Date/Place of Birth:	March, 26th 1988 in Vöcklabruck, Austria
Nationality:	Austrian
Marital Status:	Unmarried

Education

9/2010 - 11/2011	Diploma Thesis at the Linz Institute for Organic Solar Cells (LIOS)
10/2006 - 7/2010	Johannes Kepler University Linz, Austria
	Economics/Chemical Engineering, Technical Chemistry
6/2006	School Leaving Exam passed with Distinction

Language and Computer Skills

Language:	German (mother tongue), English (fluent), French (advanced), Latin (advanced)
Computer:	Microsoft Office (Word, Excel, Power Point), InkScape,
	ChemSketch, LateX/LYX, Origin

Special Training and Relevant Occupational Experience

8/2008 - 9/2008	Internship at VOEST alpine, Institute for Research and Development,
	Project: "Elimination of boron and nickel form FeO_x"
7/2009 - 9/2009	Internship at the Linz Institute for Organic Solar Cells (LIOS),
	Project: "Transistors using AlO_x"
8/2010 - 9/2010	Internship at VOEST alpine, Institute for Research and Development,
	Project: "New Biofuels"

Interests

Fabrication and research in natural, biodegradable Cosmetics,
  Travelling, Sports (Wakeboarding, Snowboarding, Skiing,...)

Eidesstattliche Erklärung

Ich erkläre an Eides statt, dass ich die vorliegende Diplomarbeit selbstständig verfasst und keine anderen als die angegebenen Quellen und Hilfsmittel benutzt habe.

Linz, den   ....
                                             (Unterschrift)